New potentialities of the Liège intranuclear cascade model for reactions induced by nucleons and light charged particles

A. Boudard,[1] J. Cugnon,[2] J.-C. David,[1] S. Leray,[1] and D. Mancusi[1]

[1]*Irfu/SPhN, CEA/Saclay, F-91191 Gif-sur-Yvette Cedex, France*

[2]*University of Liège, AGO Department, allée du 6 Août 17, bât.B 5, B-4000 LIEGE 1, Belgium*

The new version (INCL4.6) of the Liège intranuclear cascade (INC) model for the description of spallation reactions is presented in detail. Compared to the standard version (INCL4.2), it incorporates several new features, the most important of which are: (i) the inclusion of cluster production through a dynamical phase space coalescence model, (ii) the Coulomb deflection for entering and outgoing charged particles, (iii) the improvement of the treatment of Pauli blocking and of soft collisions, (iv) the introduction of experimental threshold values for the emission of particles, (v) the improvement of pion dynamics, (vi) a detailed procedure for the treatment of light-cluster-induced reactions taking care of the effects of binding energy of the nucleons inside the incident cluster and of the possible fusion reaction at low energy. Performances of the new model concerning nucleon-induced reactions are illustrated by a comparison with experimental data covering total reaction cross sections, neutron, proton, pion, and composite double-differential cross-sections, neutron multiplicities, residue mass and charge distributions, and residue recoil velocity distributions. Whenever necessary, the INCL4.6 model is coupled to the ABLA07 de-excitation model and the respective merits of the two models are then tentatively disentangled. Good agreement is generally obtained in the 200 MeV to 2 GeV range. Below 200 MeV and down to a few tens of MeV, the total reaction cross section is well reproduced and differential cross sections are reasonably well described. The model is also tested for light-ion induced reactions at low energy, below 100 MeV incident energy per nucleon. Beyond presenting the update of the INCL4.2 model, attention has been paid to applications of the new model to three topics for which some particular aspects are discussed for the first time. The first topic is the production of clusters heavier than alpha particle. It is shown that the energy spectra of these produced clusters are consistent with coalescence. The second topic regards the longitudinal residue recoil velocity and its fluctuations. Excellent results are obtained for these quantities. It addition, it is shown that the distributions of these quantities display typical random-walk characteristics, at least for not-too-large mass losses. They are interpreted as a direct consequence of the independence of successive binary collisions occurring during the cascade process. The last topic concerns the total reaction cross section and the residue-production cross sections for low-energy incident light ions. It is shown that our new model can give a rather satisfactory account of these cross sections, offering so an alternative to fusion models and the advantage of a single model for the progressive change from fusion to pre-equilibrium mechanisms.

I. INTRODUCTION

It is largely accepted that nucleon-induced spallation reactions proceed through a two-stage process: a first stage dominated by hard nucleon-nucleon (NN) collisions emitting fast particles, followed by the de-excitation of a more-or-less thermalized remnant, akin to evaporation and/or fission. The commonly used tools to describe these reactions result from the coupling of an intranuclear cascade (INC) model for the first stage to an evaporation-fission model for the second stage. There exist many INC and de-excitation models, differing from each other by the ingredients and by the results. In the last years, there has been a very strong development of applications involving spallation reactions, including neutron sources for condensed matter and material studies [1], transmutation of nuclear waste [2,3], simulation of experimental setups in nuclear and particle physics [4], production of rare isotopes [5], protection against radiation near accelerators and in space missions [6], interaction of cosmic rays in the atmosphere [7] and cancer hadron therapy [8]. This activity is at the origin of a strong demand for the improvement of the accuracy of

the reaction models and for reliable data to benchmark these models efficiently. Indeed, in Europe, an important effort has been devoted in the last fifteen years to collect and produce high-quality data concerning all emission channels: neutrons, light charged particles (lcps) and residues [9,10]. Meanwhile, model developers have constantly attempted to improve their models. We are interested here in the development of the Liège INC model (INCL4). The first standard version (INCL4.2) is described extensively in Ref. [11]. Coupled with the ABLA evaporation-fission model [12–14] (actually the KHSv3p version), it is able to describe fairly well a large body of experimental data in the 200 MeV to 2 GeV range; namely, total reaction cross sections, double-differential proton, neutron, and pion production cross sections, residue mass and charge spectra, isotopic distributions, and, to some extent, recoil energies [11]. This was achieved without any parameter adjustment in the INC model and with the use of standard values for the parameters of the ABLA model. More precisely, there is no fitting parameter in the INCL4.2 model. The basic nuclear-physics parameters, like the radius and the diffuseness

of nuclei, are taken from phenomenology and "technical parameters," like those used to evaluate phase-space occupation entering the Pauli blockers, have been fixed once for all. In addition, the stopping time is generated self-consistently by the model itself. Nevertheless, the results obtained with INCL4.2 show some systematic shortcomings and/or discrepancies with experimental data. They have been identified in the frame of the European HINDAS and NUDATRA collaborations [9,10] and are shortly presented below. The most important of these shortcomings is the inability of INCL4.2 to produce lcps (except protons of course). Since the release of the INCL4.2 model, a constant effort has been made to palliate its deficiencies.

It is the purpose of this paper to set out the present status of the INCL4 model, which is designated INCL4.6. The various points of improvements are described below. But this paper is not a mere update of the INCL model. It highlights at least three innovative points concerning spallation reactions and bearing on (i) production of clusters in the cascade, (ii) residue recoil velocities, and (iii) the behavior of the model at low energy, respectively. Concerning the first point, a dynamical coalescence model has been implemented to allow the emission of clusters in the cascade stage. An intermediate version of our model [15], sometimes denoted as INCL4.3, consisting basically of INCL4.2 plus the treatment of the emission of light clusters up to alpha particles, has opened the path to the improvement along this line. We report here on the continuation of this effort and we show that emission of heavier clusters (in practice, up to $A = 8$) can be explained by dynamical coalescence. Concerning point (ii), we show below that we are now able to reproduce average values and standard deviations of the residue-velocity distributions. Finally, let us come to point (iii). It is generally stated that INC models cannot be reliable below ∼200 MeV incident energy, although in some cases where such models are used, they occasionally give surprisingly satisfactory results. In the last years, we have tentatively but systematically improved the model in this energy range. We considerably improved the model concerning reactions induced by nucleons and by light clusters of nucleons, typically from deuterons to alpha particles, and this for incident energies per nucleon down to a few MeV. Our model is now able to produce good total reaction cross sections for both incident nucleons and incident light clusters. In addition, we show below that we are reproducing reasonably well residue-production cross sections for cluster-induced reactions at low energy. The developments concerning the three above-mentioned points were motivated in part by studies of thick targets, concerning release of volatile elements such as H and He isotopes [point (i)], radiation damages [point (ii)], and radiotoxicity [point (iii)]. Sometimes, the latter may crucially depend on secondary reactions induced by light clusters produced in primary collisions [16].

The predictive power of this improved model is considerably better than that of INCL4.2. This has been verified on an intermediate version (named INCL4.5, which is not very different from INCL4.6 and is defined below) in the course of an intercomparison of spallation codes organized by the International Atomic Energy Agency (IAEA) [17–19]. As one may surmise, the passage from INCL4.2 to INCL4.6 (even to INCL4.5) could not have been done entirely in the

same spirit of the building of INCL4.2; that is, resting on known phenomenology with well-determined parameters. We were forced to introduce less-well established features with less-solidly-determined parameters. The purpose of this paper is to present all the new features that have been introduced in INCL4.6 and to give, whenever possible, the physics motivation for these new features. Although a lot of results with INCL4.5 are available in Ref. [17], perhaps not sufficiently commented or detailed, we present here the most important results, especially to illustrate the physics aspects of the improvements brought to the model.

The paper is divided as follows: In Sec. II, we describe the INCL model with emphasis on the new features of INCL4.6. Section III is devoted to an extensive comparison with a representative panel of experimental data for nucleon-induced reactions. In Sec. IV, we discuss theoretical results for light-cluster-induced reactions concerning a few key experiments. Finally, in Sec. V, we critically examine the new features and their effects and we present our conclusion.

II. DESCRIPTION OF INCL4.6 MODEL

A. Short reminder of INCL4.2 model

The INCL4.2 model is extensively described in Ref. [11]. It is sufficient here to remind the reader of the salient features. The INCL4 model is a time-like intranuclear cascade model. In the initial state, all nucleons are prepared in phase space. Target nucleons are given position and momentum at random in agreement with Saxon-Woods and Fermi sphere distributions, respectively. They are moving in a constant potential well, the same for protons and neutrons, describing the nuclear mean field. The incident particle (nucleon or pion) is given the appropriate energy and an impact parameter at random. All nucleons are then set into motion and followed in space-time. The cascade process involves binary collisions between nucleons and produced pions and delta resonances. Particles can be transmitted through or reflected from the surface of the square-well potential they feel. Delta resonances decay according to their lifetime. Details on collisions, utilized cross sections, Pauli blocking, etc., may be found in Ref. [11] and previous publications cited therein. We recall that the stopping time of the cascade is determined self-consistently by the model itself. It can simply be parametrized (in fm/c) by

$$t_{\text{stop}} = 29.8 A_T^{0.16}, \tag{1}$$

for incident nucleons(we denote by Z_T and A_T the charge and mass numbers of the target, respectively).

It is useful to recall some other specific features which may be of importance for the rest of the paper. At the beginning of the cascade process, the incident nucleon or pion is located with its own impact parameter on the surface of the "working sphere," which is centered on the target with a radius

$$R_{\text{max}} = R_0 + 8a, \tag{2}$$

where R_0 and a are respectively the radius and the diffuseness of the target nucleus density. Particles are moving along straight-line trajectories between collisions inside the working sphere. They are divided into participants and spectators in the

usual sense. When participants leave the working sphere, they are considered as ejectiles and do not interact any more. Nucleons are moving in a potential well with constant depth and with a radius which is dependent upon their momentum. The potential radius for particles with energy larger than the Fermi energy is also taken to be equal to R_{max}. Pions do not experience any potential. Motivation and details are given in Ref. [11].

The INCL4.2 model can accommodate light clusters (up to α particles) as projectiles. In this case, the nucleons are given initially position and momentum inside the cluster and the latter is positioned at the beginning in such a way that one of its nucleons is touching the working sphere. See Ref. [11] for detail.

We comment a little bit on soft NN collisions. The latter do not contribute very much to the ejection of particles in the cascade. There are several arguments based on nuclear transport theory indicating that these collisions should be disregarded, since they induce slow modifications of the particle density distribution, a feature that is supposedly taken into account by the average nuclear potential [20–24]. In INCL4.2, soft NN collisions, with c.m. energy smaller than $\sqrt{s_0} = 1925$ MeV, are simply disregarded. This cutoff value may seem to be rather large, but one has to realize that low-energy NN collisions are largely Pauli blocked in spallation reactions. Lowering the value of $\sqrt{s_0}$ does not significantly change the results at high incident energy. It is no longer the case at low energy, say below $\sim$200 MeV, as discussed in Ref. [25]. This matter will be reexamined in this paper.

B. Shortcomings of INCL4.2 model

The shortcomings of the INCL4.2 model have been identified in various places [9–11]. We just recall them very briefly. Some phenomenological aspects of nuclear physics are neglected. The model cannot accommodate production of clusters in the cascade (i.e., with a kinetic energy definitely larger than the typical evaporation energies), as can be seen experimentally. Concerning the predictive power of the model, several deficiencies can be noted. Pion production is generally overestimated. Quasi-elastic peaks in (p, n) reactions are generally too narrow and sometimes underestimated. Finally, reaction cross sections are severely underpredicted below $\sim$100 MeV. Residue production cross sections are sometimes unsatisfactorily reproduced, especially for residues close to the target. For a matter of convenience, we separate below the new features of the INCL4.6 model into those which are included in the intermediate INCL4.5 version and those which are posterior to this version.

C. Main new features in INCL4.5 model

1. Introduction of known phenomenology

a. Isospin and energy-dependent potential well for the nucleons. The depth of the potential well felt by the nucleons is dependent on the energy of the nucleons and is not the same for protons and neutrons. The energy dependence is taken from the phenomenology of the real part of the optical-model potential [26–28]. Roughly speaking, the potential depth decreases regularly with increasing energy, from ordinary

values at the Fermi level to zero at roughly 200 MeV. The isospin dependence is such that the neutron and proton Fermi levels have the same energy. For more detail, see Ref. [29]. The influence of this modification is relatively small, except for special quantities, like the production cross sections for isotopes with an extra unit of charge compared to the target [29,30].

b. Average potential for pions. An average isospin-dependent potential well of the Lane type [31] is introduced for pions, as well as reflection and/or transmission at the border of this potential. The depth of the potential has been taken, as far as possible, from the phenomenology of the real part of the pion-nucleus optical potential (dispersive effects due to the strong imaginary part have to be removed). This depth amounts to 22 MeV for π^+ and 38 MeV for π^- on a Pb target. The radius of the potential is taken as $R_0 + 4a$, in rough accordance with phenomenology. This modification and its effect are presented in detail in Ref. [32]. In general, it reduces the pion production cross section, thereby mitigating the overestimate by INCL4.2, as illustrated below by Fig. 11.

c. Deflection of charged particles in the Coulomb field. Once an impact parameter is selected for the incident nucleon, the cascade process is initiated with this nucleon located at the intersection of the "external" Coulomb trajectory (corresponding asymptotically to the specific impact parameter) with the "working sphere" (see above). The same procedure is used to connect the direction of an outgoing particle at the nuclear periphery and its asymptotic direction.

These three modifications can be considered as mandatory. They do not introduce any fitting parameter. Values of the parameters have been fixed once for all, largely inspired from known phenomenology.

2. Emission of clusters

An improvement of the INCL4.2 model concerning this feature had been already proposed in Ref. [15]. The implementation of this feature in INCL4.5 is somehow different, although the basic idea is the same: an outgoing nucleon crossing the nuclear periphery is supposed to be able to carry along other nucleons to form a cluster, provided the involved nucleons are lying sufficiently near each other in phase space. We first describe the present implementation in INCL4.5 and then comment upon the difference with the work of Ref. [15].

The features of the model for cluster production can be described as follows:

(i) An outgoing nucleon arriving at the surface of the "working sphere," whether or not it has made collisions earlier, is selected as a possible leading nucleon for cluster emission, provided its energy is larger than the threshold energy, otherwise it is reflected.

(ii) Potential clusters are then constructed. The leading nucleon is drawn on its (straight) line of motion back to a radial distance

$$D = R_0 + h, \tag{3}$$

with R_0 being the half-density radius, and clusters are built by searching nucleons which are sufficiently

Z\N	1	2	3	4	5	6	7	8	9
8				2p				^{16}O	^{17}O
7			p	p	11 ms		^{14}N	^{15}N	
6		2p	0.13 s	19 s	0.33 h	^{12}C	^{13}C		
5		2p	0.77 s	p	^{10}B	^{11}B	20 ms		
4		2p	53 d	α	^{9}Be	$1.6\ 10^6$ yr	13.8 s	24 ms	
3	p	p	^{6}Li	^{7}Li	0.84 s	0.18 s	n	8.5 ms	n
2	^{3}He	^{4}He	n	0.8 s	n	0.12 s	n	2n	
1	^{2}H	12.3 yr	n	2n	n	2n			
Z/N	1	2	3	4	5	6	7	8	9

FIG. 1. (Color online) In this graph, the considered clusters for $A_{\rm cl}^{\rm max} = 12$ are identified by their charge Z (vertical ordering) and neutron N (horizontal ordering) numbers and are displayed inside the perimeter delineated by the heavy line. Absolutely stable clusters are denoted by the ordinary symbols inside yellow cells. Cells displaying a time correspond to clusters with a lifetime larger than 1 ms, which are considered as detectable clusters. Other cells (in blue) correspond to clusters with a lifetime smaller than 1 ms. They are forced to decay by the indicated mode.

close in phase space (Δs are excluded).[1] Clusters of increasing sizes are built successively. All potential clusters up to a maximum size $A_{\rm cl}^{\rm max}$ are considered. The criterion of sufficient proximity is expressed with the help of Jacobian coordinates:

$$r_{i,[i-1]}\, p_{i,[i-1]} \leqslant h_0(A_{\rm cl}) \quad \text{for } i = 2, 3, \ldots, A_{\rm cl}, \qquad (4)$$

where $r_{i,[i-1]}$ and $p_{i,[i-1]}$ are the relative coordinates of ith nucleon with respect to the subgroup constituted of the first $[i-1]$ nucleons ($i = 1$ corresponding to the leading nucleon) and where $A_{\rm cl}$ is the mass number of the cluster. The value of $h_0(A_{\rm cl})$ is discussed below. The test on Jacobian coordinates is preferred to the usual test on the relative coordinates r_{ij}, p_{ij} for any pair (i, j) of particles, because it disfavours exotic shapes (such as spaghetti) of the clusters. Considered clusters up to $A_{\rm cl}^{\rm max} = 12$ are listed in Fig. 1. For the moment, due to extremely fast increase of the combinatorics with the mass of the cluster and due to limitations in computing time, clusters up to $A_{\rm cl}^{\rm max} = 8$ are considered. Extending $A_{\rm cl}^{\rm max}$ beyond this value may change the yields. We have checked that problems of convergence of the procedure manifest themselves by a slight excess of the yield for clusters with mass number equal to $A_{\rm cl}^{\rm max}$, as indicated in Ref. [33], so that in practice numerically stable results are obtained for clusters of mass up to 7, and that the predicted yield for production of mass 8 can be considered as an upper bound.

(iii) The less "virtual" cluster is selected. Let $\sqrt{s}$ be the c.m. energy of the composing nucleons, built on the four-momentum of a cluster, defined as the sum of the four-momenta of the nucleons inside the cluster. Let us consider the quantity

$$\nu = \left(\sqrt{s} - \sum m_i\right) A_{\rm cl} - B_{\rm cl}/A_{\rm cl}, \qquad (5)$$

where $B_{\rm cl}$ is the (nominal) binding energy of the cluster. The cluster with the minimum value of ν is selected.

This quantity can be viewed as the excitation energy per nucleon of the cluster diminished by twice the binding energy per nucleon. The introduction of this quantity is largely phenomenological and is solely justified by the relative success of the model.

(iv) The selected cluster is emitted provided three conditions are satisfied. First, it should have sufficient energy to escape; that is, $T_{\rm cl} = \sum(T_i - V_i) - B_{\rm cl} > 0$, where the T_i are the kinetic energies of the nucleons and where the V_i are the depths of their potential wells. Second, the cluster also has to succeed the test for penetration through the Coulomb barrier. Third, the cluster cannot be emitted too tangentially. If θ is the angle between the direction of the cluster (defined as the direction of its total three-momentum) and the radial outward direction passing by the center of mass of the potential cluster, it is required that

$$\cos\theta > 0.7. \qquad (6)$$

The idea behind this condition is that when a nascent cluster spends too much time in the nuclear surface, it likely gets dissolved. These choices are admittedly made to improve the results at low energy, although some supporting arguments can be produced.

(v) If these tests are successful, the cluster is emitted with the kinetic energy $T_{\rm cl}$ in the direction of the total momentum of its components. If they are not, the leading nucleon is emitted alone provided it succeeds the test for penetration of the Coulomb barrier. If not, the leading nucleon is simply reflected.

(vi) At the end of the cascade process, short-lived clusters with a lifetime less than 1 ms (e.g., ^{5}Li) are forced to decay isotropically in their c.m. frame. Clusters with a lifetime larger than 1 ms are considered detectable as such, prior to decay. Details are summarized in Fig. 1.

In our previous work [15], which was primarily devoted to production of clusters (up to $A_{\rm cl} = 4$) at high energy (i.e., from 500 to 2500 MeV), two parameters, h [Eq. (3)] and a single parameter h_0 for all clusters in Eq. (4), with the selection of the heaviest-possible cluster, were sufficient. In order to have a more-or-less satisfactory description at low energy, we have been forced to consider different values of the parameter h_0 for light clusters ($A_{\rm cl} \leqslant 4$) and a simple law [$h_0 = h_1(A_{\rm cl}/5)^{1/3}$] for heavier clusters. In INCL4.5, the parameters have been determined once for all by fitting data to a few illustrative cases. The values of the parameters are given in Table I.

TABLE I. Values of parameters of cluster-formation model. The parameters are described in the text: h is given in fm, h_0 and h_1 are given in fm MeV/c.

h	h_0 (2)	h_0 (3)	h_0 (4)	h_1 ($A_{\rm cl} > 4$)
1.0	424	300	300	359

---

[1]If the line of motion of the nucleon does not cross the sphere of radius $R_0 + h$, the nucleon is moved back to the minimum distance of approach of the center of the nucleus.

3. Modifications concerning Pauli blocking

A strict Pauli blocking is applied to the first collision: the nucleons should lie outside the Fermi sea after the first collision. In INCL4.2, the Pauli blocking is applied stochastically, according to the product of the final-state blocking factors. Conjugated with the fact that constructing the target with nucleons at random generates events with a nonuniform Fermi sea (even if it is uniform on the average over events), this procedure has the drawback of sometimes allowing collisions which otherwise (i.e., in a perfectly filled Fermi sea) would be strictly forbidden. On the other hand, it allows us to account for surface effects and for effects of the depletion of the Fermi sea as the cascade process evolves. It is found in Refs. [25,34] that a good compromise is achieved when a strict Pauli blocking is adopted for the first collision and when the usual procedure is kept for the subsequent collisions.

4. Modifications for soft collisions

a. Soft collisions. In INCL4.2, soft collisions (with c.m. energy $\sqrt{s} < \sqrt{s_0} = 1925$ MeV) are neglected. Historically, this choice was made to avoid inconveniences linked with the raising NN cross sections at low energy. More profoundly, the underlying argument states that soft collisions (with low momentum transfer) do not change significantly the energy-momentum flow in the system and that their effect is likely to be more reasonably accounted for by the nuclear mean field. Furthermore, changing the boundary between soft and hard collisions has no sharp effect. The reason is that, in spallation reactions, soft collisions occur mainly when the colliding nucleons are lying close to the Fermi energy and thus that these collisions are largely Pauli blocked, as explained in Ref. [34]. This argument breaks down when a low-energy incident nucleon makes a collision in the nuclear periphery, where Pauli blocking is not very efficient. We thus decided to lower $\sqrt{s_0}$, still trying to keep the results roughly equivalent and to save computation time. The new value is now $\sqrt{s_0} = 1910$ MeV.

b. Special treatment of first collision. For the first collision, we even lowered the value of $\sqrt{s_0}$ to the minimum (i.e., twice the nucleon mass), in apparent contradiction with the arguments above. However, at low energy, only a few (1 to 3, on the average) collisions occur. Neglecting a soft collision, allowed however by Pauli blocking, especially the first one, may amount to neglecting the event. This may have dramatic effects on the total reaction cross section, since the latter involves all kinds of events, be them hard or soft. It should be stressed that this procedure does not change the results at high energy (say, above ~200 MeV). Indeed, in this case, the first collision is always a hard one. Neglecting a subsequent soft collision is harmless most of the time. See Ref. [35] for more details. In addition, a special procedure, named "local E," is applied to the first collision. In INCL4.2, the momenta of the target nucleons are too large at the nuclear surface, near the turning points, since they experience constant square-well potentials, instead of smoothly varying potentials (this is "the price to pay" to keep the simplicity of straight-line motion in our code, see Ref. [11] for details). In the local E procedure, when two nucleons are selected for the first collision, their

momenta are "corrected" by replacing their values with those assumed by the nucleons in a smoothly varying potential at the same positions. When testing a pair of nucleons for collision, the NN cross section is calculated with the corrected momenta. After the collision, if it occurs, momenta are "corrected back" to the INCL4.2 prescription. Once again, this procedure has no effect on the first collision at high incident energy, nor when this first collision occurs in the bulk of the target nucleus. These two modifications are instrumental to give the predictions of the total reaction cross section in agreement with experimental data at low energy.

5. Modification of status of participants

If after a binary collision or after a Δ decay, a nucleon (obviously a participant) has an energy smaller than the Fermi energy plus a small quantity ξ, put arbitrarily equal to 18 MeV as a first attempt, it is considered thereafter as a spectator (it can be "repromoted" as a participant if it gets a sufficiently large energy transfer in a subsequent collision with a participant). This procedure, which is inspired from the ISABEL code [36–38], may be motivated by various considerations: in a nucleus, the Fermi sea is not sharply defined, nucleons cannot be localized with precision when their energy is low and correlations may render the difference between a nucleon above the Fermi level and a spectator rather fuzzy. In fact, there is no compelling argument in favour of this procedure. It is included here because it gives slightly better results in some cases, in particular for production of clusters at low incident energy. Unfortunately, it leads, in our case, to unphysical results in neutron spectra at very low incident energy, as clearly illustrated in Fig. 5 below. That is why this feature has been changed in the INCL4.6 version, see below. For convenience, we will refer to this procedure as the "back-to-spectator" recipe.

D. Additional features included in INCL4.6 model

1. Further modification of status of participants

As just stated above, the modification described in Sec. II C5 produces unpleasant results in neutron- and proton-energy spectra, which will be illustrated when discussing comparisons with experimental data. In INCL4.6, participant neutrons are considered as spectators when their energy gets below the neutron-emission threshold, corresponding roughly to ξ defined above and equal to 7 MeV. The same procedure is adopted for participant protons when their energy falls below their emission threshold plus two thirds of their Coulomb barrier. The whole procedure is certainly more acceptable, although it is not really justified on consistency arguments, but it is validated *a posteriori* by the results, as shown below (see Figs. 5 and 6).

2. Use of experimental thresholds for nucleon emission

In our standard model, a participant nucleon (of type $i = n, p$) can be emitted when it hits the surface of the potential with a kinetic energy E larger than the potential depth, or equivalently when the difference of energy E with the Fermi

energy, $E - E_F^i$, is larger than the model separation energy S_i. If it is emitted, the nucleon acquires an asymptotic kinetic energy E_∞ given by

$$E_\infty = E - E_F^i - S_i. \tag{7}$$

In our standard model, the values of S_i are fixed for a given target nucleus and equal to the differences between the potential depths and the Fermi energies, respectively.[2] In INCL4.6, the energy $E - E_F^i$ is compared to the physical separation energy S_i^{phys}, taken from mass tables, for the emission from the actual nucleus (i.e., the target nucleus left over when the candidate particle is hitting the surface). Equation (7) is replaced by

$$E_\infty = E - E_F^i - S_i^{\text{phys}}. \tag{8}$$

The effect is expectedly small, except at low incident energy, where the precise value of the threshold energy for a reaction does matter, or when the evolution of the target in the course of the cascade reaches the border of available phase space.

3. Modified value for $R_{\max}$

Using a value given by Eq. (2) for the radius for the "working sphere" of $R_{\max} = R_0 + 8a$ is safe at high energy, since this value allows a sampling of impact parameters concerning all reaction events: it encompasses the outskirts of the nuclear density by a value which is greater than $r_{\text{int}} = (\sigma_{NN}^{\text{tot}}/\pi)^{1/2}$, which we denote for simplicity as the "range of interaction," σ_{NN}^{tot} being the NN total cross section at the incident energy per nucleon.[3] This is no longer true at low energy (from a few MeV to a few tens of MeV), where the range of interaction may become very large, because of the rising NN cross sections. We thus decided to use

$$R_{\max} = R_0 + 8a + r_{\text{int}} = R_1 + 8a. \tag{9}$$

Accordingly, we have increased the maximum time of the cascade, which now corresponds to the time of passage of the incident particle through the "working sphere" along a diameter, when this time exceeds the usual stopping time, given by Eq. (1).

4. Treatment of cluster-induced reactions

In INCL4.2, an incident cluster (up to an alpha particle) is considered as a collection of independent nucleons with internal Fermi motion superimposed on the motion of the incident cluster as a whole (see Ref. [11]), adjusted in such a way that the sum of the total energies of the constituting nucleons is equal to the nominal energy of the physical cluster. In other words, the cluster is replaced by independent

on-shell nucleons with the correct nominal total energy, but with an incorrect (smaller than nominal) total momentum. This approximation is justified at high energy, where the missing momentum is relatively small, and where this model gives more-or-less satisfactory results [11,39,40]. However, it is not really appropriate for reactions at low incident energy. In this domain, several features should be taken properly. First the total energy-momentum content of the projectile should be preserved. Second, the collective motion of the projectile has to be respected at low energy and Fermi motion has to be progressively restored when the available energy allows it. Liberating Fermi motion at a too-early stage (as in INCL4.2) may be harmful at low energy. Indeed, for a nucleon with a backward-oriented Fermi motion velocity larger than the collective velocity, the projectile may fly at once in the backward direction, which is indeed unphysical. Third, emission of projectile spectators with the influence of their Fermi motion should be possible and dominated by geometrical properties. This property, which is well established at high energy [41–43], is expected to survive, to some extent, at low energy, at least for large impact parameters. Finally, compound-nucleus formation should dominate at low incident energy. To fulfill these requirements, we have implemented an ad hoc model made of the following ingredients:

a. Initialization of incident cluster. Nucleon momenta $\vec{p}_i'$ and positions $\vec{r}_i'$ inside the cluster are generated as before [11] (note, however, that a special method is applied to ensure $\sum \vec{p}_i' = 0$ and $\sum \vec{r}_i' = 0$). At the beginning of the event, the cluster center of mass is positioned on the classical Coulomb trajectory in such a way that one of the nucleons is touching a sphere of radius R_{Coul}. The latter represents the Coulomb barrier. The value of R_{Coul} is taken from the phenomenology of the Coulomb-barrier heights and has been tabulated as function of the target mass for p, d, t, ^{3}He, and ^{4}He projectiles. It is given in the appendix. Of course, for very large impact parameters and/or low incident energy, the Coulomb trajectory may miss the sphere of radius R_{Coul}. The incident cluster is then positioned at the minimum distance of approach.

For the energy-momentum content, the following procedure is adopted: Let e_i' and $\vec{p}_i'$, be the energy and the momentum of the nucleons generated (as in INCL4.2) in the frame of the incident cluster [one has $e_i' = (\vec{p}_i'^2 + m_i^2)^{1/2}$, $\sum \vec{p}_i' = 0$]. The nucleons are put off shell by changing their energy e_i' into $e_i = e_i' - v$, defined by

$$\sum e_i = \sum (e_i' - v) = M_{\text{inc}}, \tag{10}$$

where M_{inc} is the exact projectile mass. When Lorentz boosted with the incident velocity $\vec{\beta}_{\text{inc}} = \vec{P}_{\text{inc}}/M_{\text{inc}}$, with $\vec{P}_{\text{inc}}$ being the nominal momentum of the projectile, the nucleons acquire four-momenta $(E_i, \vec{p}_i)$ such that

$$\sum E_i = W_{\text{inc}}, \qquad \sum \vec{p}_i = \vec{P}_{\text{inc}}, \tag{11}$$

where W_{inc} is the exact total energy of the projectile. This rather crude procedure aims at preserving the energy-momentum content of the cluster when replacing it by nucleons. The latter are then off shell, which naturally accounts for their binding. Naively, the quantity v can be viewed as the potential necessary to bind the nucleons to the right binding energy of

---

[2]The definition of S_i is slightly more involved for energy-dependent potentials. We simplify the presentation on this minor point.

[3]In INCL, collisions are decided on a minimum of relative distance basis, which is equivalent to introducing an effective interaction with a range equal to r_{int}.

the cluster. At large incident cluster energy, the four-momenta of the nucleons inside the projectile are basically the same in the two schemes.

b. Generation of geometrical spectators. When positioned as indicated above, the nucleons of the projectile are separated into geometrical participants and geometrical spectators, which are those nucleons whose direction of motion intercepts (or not) the working sphere, respectively.[4] To perform this separation, the direction of motion of the nucleons is assumed to be parallel to the collective velocity vector of the cluster. Spectator nucleons are put on shell with momentum $\vec{p}_i$, defined above, and energy $E_i^{\text{spec}} = (\vec{p}_i^{\,2} + m_i^2)^{1/2}$, and are frozen further on. In order to preserve the correct energy balance, the energy of the participants are decreased correlatively and equally.

c. Treatment of geometrical participants. The following criteria are used: If a participant has an energy lower than the bottom of the target potential well, the event is discarded. This happens very rarely when, due to fluctuations, the generated Fermi motion energy is very small, but occurs close to thresholds for emissions of particles.

If all the geometrical participant nucleons have a total energy above the bottom of the target potential and if one of these nucleons has a trajectory cutting the sphere of radius R_1 defined in Eq. (9) and if one of these nucleons at least has an energy *below* the Fermi energy, a compound nucleus is formed with all the geometrical participants and the target, with an energy which is equal to the available energy. The thus-constructed compound nucleus is ready for de-excitation (no further cascade is performed). Of course, its energy should be larger than the nominal ground-state energy, otherwise the event is discarded. This choice is inspired by the fact that a compound nucleus is expectedly formed at low energy when the inhibiting effects of the Coulomb barrier are overcome.

Finally, when all the geometrical participants have an energy above the Fermi energy, the usual cascade is applied. However, before colliding for the first time, geometrical participants are propagated with the velocity of the incident cluster as a whole. Right before their first collision, they are given back their Fermi motion and are put on shell. We take Fermi motion into account for calculating the cross section and the kinematics of the collision.

d. Coulomb polarization of incident deuterons. When an incident deuteron is selected, it is positioned initially with one of its nucleons touching the sphere of radius R_{Coul}. For heavy targets, if this nucleon is a proton, it is interchanged with the neutron. This procedure mocks up the polarization of the deuteron by the Coulomb field of the target. It is often advocated that this effect is necessary to properly describe deuteron-induced reactions [44].

The model described above may appear as a rather ad hoc procedure. It has been inspired by our willingness of

_____

[4]This "geometrical spectator" term is used to distinguish these spectators, which are defined here by a geometrical criterion, from the usual definition of the spectators that are those nucleons, which, in a true reaction event, are intercepting the target, but avoid, by chance, collisions.

coping with several aspects of the low-energy dynamics. But it can compete with other models, such as fusion models. It manages Coulomb effects and Fermi blocking effects at low energy but, in addition, it leads automatically and dynamically to departures from compound-nucleus formation as the incident energy increases. Of course, we are well aware of the fact that a valid justification of our procedure can mainly come from a successful confrontation with experimental data.

We have presented here the initializations of the nucleon-induced and cluster-induced events separately. We want to stress that these preparations are not disjoint, however. Actually, the initialization of a cluster-induced event reduces to the one of a nucleon-induced event when the cluster is reduced to a single nucleon without Fermi motion.

III. COMPARISON WITH EXPERIMENTAL DATA FOR NUCLEON-INDUCED REACTIONS

A. Introduction

We will not make a thorough comparison with experimental data, nor with the predictions of competing models, such as Bertini [45,46], Isabel [36,37], CEM03 [47,48], BUU [49], IQMD [50], JQMD [51], and the BIC cascade of Geant4 [4] (see Ref. [52] for a recent description of most of these models), since such a comparison can be found in the IAEA Intercomparison [17] for INCL4.5. We will restrict ourselves to a comparison with data in cases where the influence of the modifications brought by INCL4.5 and INCL4.6 are important or when the physical significance of the modifications brought by INCL4.6 in comparison with INCL4.2 can be tested. For nucleon-induced reactions, the differences between INCL4.5 and INCL4.6 predictions are rather of minor importance, except for low-energy neutron spectra, which is illustrated in Sec. III C 2. All INCL4.5 and INCL4.6 predictions have been obtained with the adjunction of the ABLA07 de-excitation model (actually the ABLA07V5 version), described in Ref. [53].

B. Total reaction cross sections

This observable is entirely determined by the cascade stage and even by the first collision in this stage. Total reaction cross sections calculated with INCL4.2, INCL4.5, and INCL4.6 are displayed in Fig. 2. Whereas the predictions are roughly the same for the three models above 200 MeV, there is a dramatic improvement brought by INCL4.5 and especially INCL4.6 in the 10 MeV to 100 MeV range. We recall that the difference between the INCL4.5 and INCL4.6 predictions mainly comes from a too-small radius R_{max} of the working sphere in INCL4.5 which, especially at low energy, underestimates the number of interacting events for large impact parameters. It is remarkable that INCL4.6 is able to account for the bump of the cross sections appearing at a few tens of MeV and for its main properties, except for the Be target. The systematic parametrization of the data given in Ref. [54] seems to indicate that reaction cross sections are not sensitive to structure effects and are smoothly varying with incident energy and target mass
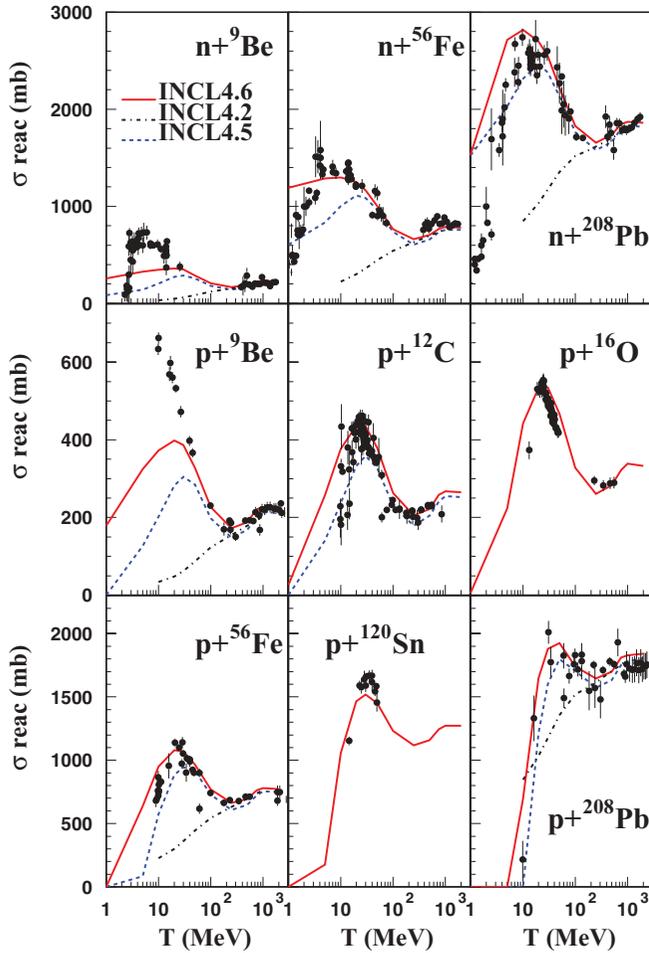
FIG. 2. (Color online) Comparison of INCL4.2 (black), INCL4.5 (blue), and INCL4.6 (red) predictions with experimental data for the total reaction cross section as a function of the incident kinetic energy T for neutron-induced reactions on ^{9}Be, ^{56}Fe, and ^{208}Pb (first row) and proton-induced reactions on ^{9}Be, ^{12}C, ^{16}O, ^{56}Fe, ^{120}Sn, and ^{208}Pb (second and third rows). Data are from Refs. [54–56].

FIG. 3. (Color online) Comparison of INCL4.2 (black dotted lines) and INCL4.5 (full red lines) predictions with experimental data for the total reaction cross section as a function of the incident kinetic energy T in various systems. Dashed red lines correspond to INCL4.6 predictions when Coulomb deflection is neglected. Dotted (dot-and-dashed) lines correspond to INCL4.6 predictions when so-called local E corrections (soft collision suppression) are neglected. See text for details. Data are taken from Refs. [54–56] and, for a given panel, may refer to several different isotopes. See these references for detail.

number, except for light nuclei at low incident energy, as it is illustrated by Fig. 2.

Above 200 MeV, where there is no real difference between the predictions of the three models, the variation of the total reaction cross section with the incident energy closely follows the variation of the NN total cross section, a feature that comes naturally in Glauber models [57] for total reaction cross section. It is interesting to look at the origin of the differences between the INCL4.2 and INCL4.5 (or 4.6) predictions below 200 MeV. This is indicated by Fig. 3, where we have compared INCL4.2 predictions with INCL4.6 predictions when one of the additional features of this latter model is removed: Coulomb deflection, removal of soft collisions, and the so-called local E correction (see above). This figure clearly shows that, in proton-induced reactions, the rise of the reaction cross section when the incident energy decreases from 200 to 30–40 MeV is due to the removal of the cut on soft collisions for the first collision, which in fact takes full account of the strong increase of the raising NN cross section with decreasing incident energy in this range, when the local E correction,

defined above, is applied. This correction alone is already giving an important increase of the cross section, as indicated by the dotted curves in Fig. 3. Of course, at very low energy, the reaction cross section for incident protons is decreased by the Coulomb repulsion, which leads to a global sharp decrease below the Coulomb barrier. In fact, it appears from Fig. 3 that it is important to take into account all the features which determine the probability of the first interaction. These effects are rather well identified in macroscopic models for the reaction cross sections [54,57]. Similar considerations can be done for neutron-induced reactions. However, in this case, the falloff of the reaction cross section at low energy is basically due, in our model, to the Pauli blocking of collisions at very low incident energy.

TABLE II. Neutron multiplicities (third column) obtained by integration of the experimental double-differential cross sections of Ref. [58] in proton-induced reactions on ^{208}Pb nuclei at three values of the incident kinetic energy T, compared with the predictions of various INCL-ABLA couplings.

Incident kinetic energy	Neutron energy	Expt.	INCL4.2 ABLA	INCL4.5 ABLA07	INCL4.6 ABLA07
800 MeV	2–20 MeV	6.5 ± 0.7	6.8	6.33	6.73
800 MeV	20 MeV–E_{max}	1.9 ± 0.2	2.5	1.84	1.91
1200 MeV	2–20 MeV	8.3 ± 0.8	8.1	7.8	8.27
1200 MeV	20 MeV–E_{max}	2.7 ± 0.3	3.1	2.39	2.48
1600 MeV	2–20 MeV	10.1 ± 1.0	8.8	8.6	9.16
1600 MeV	20 MeV–E_{max}	3.4 ± 0.5	3.7	2.79	2.90

C. Emission of light particles

1. Neutron multiplicity in cascade stage

Neutron multiplicity is of crucial importance for nuclear energy applications. For our purpose here, it is convenient, following Ref. [58], to consider the multiplicity of neutrons with a kinetic energy larger than 20 MeV, since this quantity is sensitive to the cascade stage only. Results are given in Table II. One can see that our predictions with the latest version INCL4.6 are globally satisfactory, although the agreement with experimental data is somehow marginal at 1600 MeV. The decrease of the $E > 20$ MeV neutron multiplicity from INCL4.2 to INCL4.6 is due to the back-to-spectator procedure. It can also be seen from Table II that the predicted neutron multiplicities in the 2 to 20 MeV range are rather well described. In this case, of course, the merit is to be shared by ABLA07 and INCL4.6, since the latter determines the excitation energy of the remnant, prior to evaporation.

2. Neutron energy spectra

These quantities are also of importance for applications. We will not comment very much on this point since extensive results can be found in the IAEA Intercomparison and since globally, all our models are giving rather satisfactory results for neutrons with a kinetic energy larger than 20 MeV (i.e., for those neutrons produced in the cascade stage). As an illustrative example, we show in Fig. 4 the predictions of INCL4.2 and INCL4.6 for the neutron spectra in $p + ^{208}$Pb collisions at 1200 MeV.

The INCL4.5 (not shown) and INCL4.6 models give essentially the same results, for all targets and all incident energies, except below ∼100 MeV (see below). The predictions of these models are somehow less good than those of INCL4.2. The difference particularly concerns neutrons with a kinetic energy between 20 to 50 MeV at angles between 10 and 50 degrees, where INCL4.5 and INCL4.6 underestimate the cross sections. This deficiency partly comes from the implementation of the production of composite particles by coalescence (inexistent in INCL4.2), which in a sense "eats up" neutrons and protons in this energy range, and partly from the use of energy-dependent nucleon average potentials. Note that this deficiency is reduced at 800 MeV and seems to be slightly increased for lighter
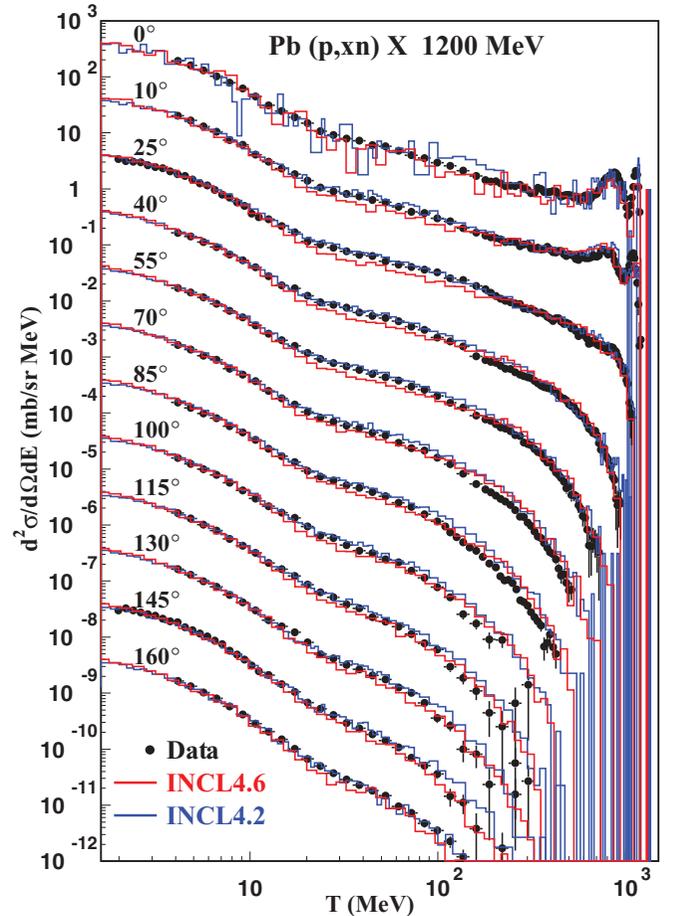
FIG. 4. (Color online) Comparison of INCL4.2 (blue) and INCL4.6 (red) predictions with experimental data for neutron double-differential cross sections in $p + ^{208}$Pb collisions at 1200 MeV, as functions of the neutron kinetic energy T and at different angles, indicated on the figure. For the sake of clarity, the various spectra have been multiplied by 10^0, 10^{-1}, 10^{-2}, etc., for increasing angles, starting at the lowest angle. Data are from Ref. [59].

targets (Fe, Zr). It can also be seen from Fig. 4 that INCL4.6 is slightly better than INCL4.2 for the high-energy part of the spectra.

We show in Fig. 5 the kind of results that we obtain around 60 MeV incident kinetic energy. The striking feature is the "dip" in the neutron spectra around 10 MeV produced by the INCL4.5 model. This originates from the back-to-spectator recipe, explained in Sec. II C5. This unphysical feature disappears in INCL4.6, since the quantity ξ is then reduced to 7 MeV for neutrons and the same quantity plus two thirds of the Coulomb-barrier height for protons. Dips are so removed from the nucleon spectra. Dips of this kind are not visible at high energy (say above 100 MeV; see, for instance, Fig. 4) because they are hidden by the overwhelming evaporation contribution. The theoretical shapes of the spectra above the evaporation peaks in Fig. 5 are rather satisfactory, although the degree of agreement is substantially smaller than at high energy (see Fig. 4). As a matter of fact, the shapes are almost perfectly reproduced at 800 MeV and are progressively departing from experiment when the incident energy is decreasing.
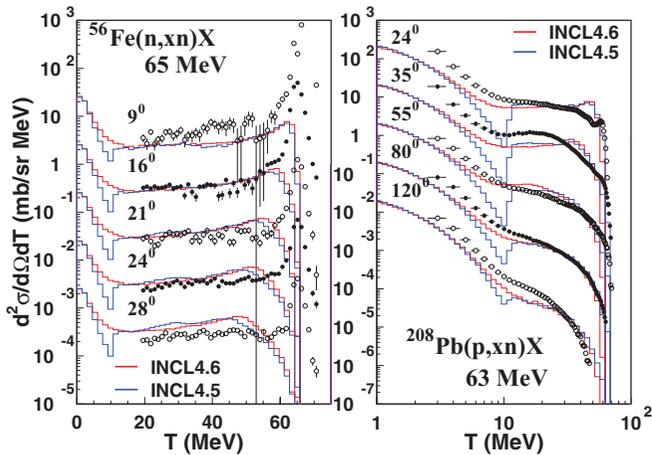
FIG. 5. (Color online) Comparison of INCL4.5 (blue) and INCL4.6 (red) predictions for the neutron double-differential cross sections in $n + {}^{56}$Fe collisions at 65 MeV (left panel, data from Ref. [60]) and in $p + {}^{208}$Pb collisions at 63 MeV (right panel, data from Ref. [61]). Same convention as in Fig. 4 for the display of the spectra.

3. Proton energy spectra

We spot some of our results in Fig. 6. Clearly, the kind of discontinuity observed in low-energy proton spectra at 62 MeV incident kinetic energy and due to the use of the back-to-spectators trick in INCL4.5 has disappeared in INCL4.6, as shown in the upper-left panel of Fig. 6.

The INCL4.6 results are globally somehow satisfactory. However, systematic deficiencies can be detected. Cross sections are overpredicted for proton energies in the 10 to ~50 MeV range at lowest angles [Fig. 6(a)], although results for heavier targets (not shown) are much better. This seems to come from an overestimate of the quasi-elastic component. Spectra at small angles and in the 40 to 100 MeV energy range are underpredicted at 175 MeV proton incident energy [Fig. 6(b)] and to a lesser extent at incident energy larger than 800 MeV [Fig. 6(d)]. This defect seems to disappear around 800 MeV [Fig. 6(c)], where the agreement with experiment is remarkable. The origin of this discrepancy is not clear since it occurs in a region of the spectrum neighboring the quasi-elastic and quasi-inelastic peaks. The latter are believed to come from a single NN collision and thus from events with a low number of collisions. It is thus surprising that our model, be it INCL4.5 or INCL4.6, is able to describe reasonably well the quasi-elastic and quasi-inelastic peaks (at least above 250 MeV) and not this few-collision component, except around 800 MeV.

Let us also mention that our calculations overestimate the proton yield in the evaporation region at high incident energy [see Fig. 6(d)]. This may point to a deficient competition between the various particle emissions in the different versions of the ABLA model (or to an incorrect excitation energy of the target in INCL4.6). Let us however recall that the spectra of evaporated neutrons, which provides the dominant channel in this energy range, are rather well described by the ABLA model, as indicated by Fig. 4.

We finally comment on the comparison with INCL4.2 (not shown here; see Ref. [11]). The predictions of the latter concerning proton spectra are slightly better at high
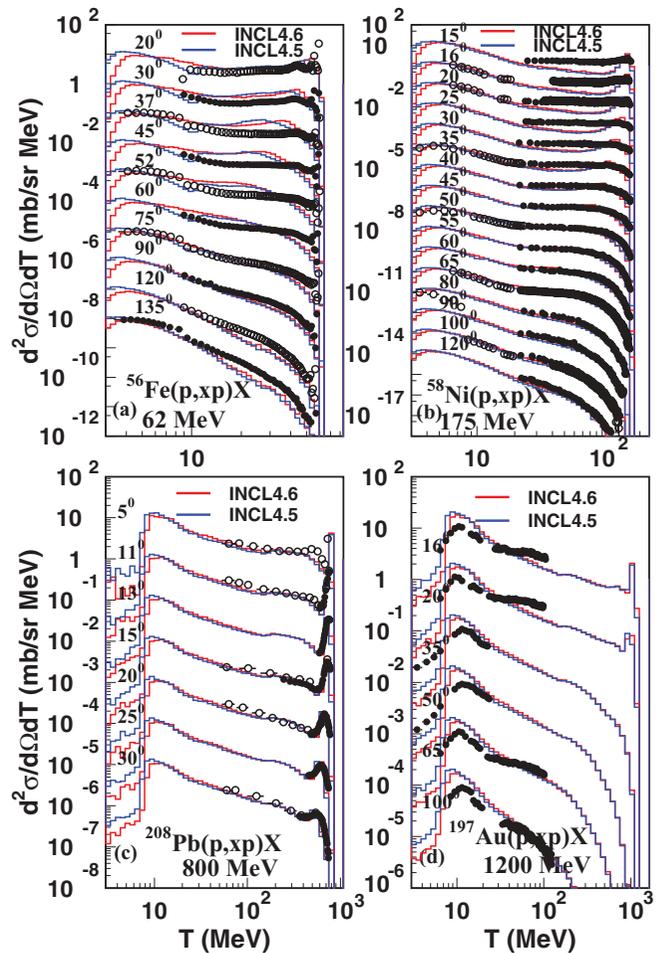
FIG. 6. (Color online) Comparison of INCL4.5 (blue) and INCL4.6 (red) predictions with the experimental data (symbols) for the proton double-differential cross sections in $p + {}^{56}$Fe collisions at 62 MeV [panel (a), data from Refs. [62,63]], in $p + {}^{58}$Ni collisions at 175 MeV [panel (b), data from Refs. [63,64]], in $p + {}^{208}$Pb collisions at 800 MeV [panel (c), data of Refs. [65,66]], and in $p + {}^{197}$Au collisions at 1200 MeV [panel (d), data of Ref. [67]]. Same convention as in Fig. 4 for the display of the spectra.

energy, with a less-pronounced deficiency at small angles and intermediate proton energy. At low incident energy, say below 150 MeV, the shape of the spectra are slightly better (see Ref. [25]), but the normalizations are noticeably lower than those of experimental data, since the total reaction cross sections are badly underestimated, as noticed in Sec. III B.

4. Light-cluster energy spectra

This is an important feature of INCL4.6, since INCL4.2 can not accommodate emission of clusters during the cascade stage. We have made extensive calculations with our new INCL4.6 model for double-differential cross sections of d, t, ^{3}He, and α production and compared with representative experimental data of Refs [61,62,64,67–72] covering a large incident energy range (62 MeV to 2.5 GeV) and a target mass range spanning from Al to Bi. Extensive results can be found
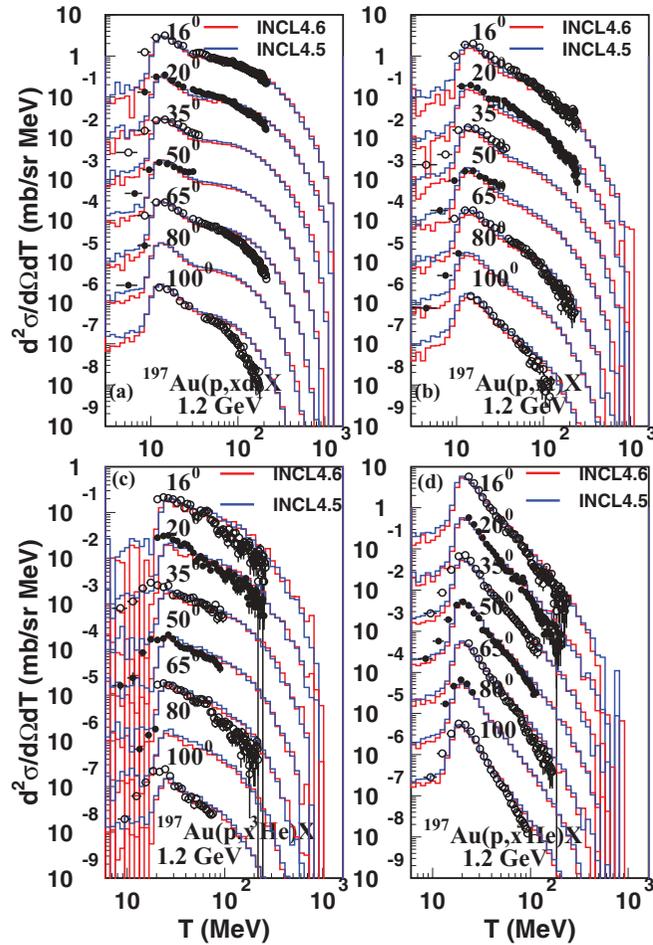
FIG. 7. (Color online) Comparison of INCL4.5 (blue) and INCL4.6 (red) predictions for the double-differential cross sections for deuteron [panel (a)], triton [panel (b)], ^{3}He [panel (c)], and ^{4}He [panel (d)] production in $p + {}^{197}$Au collisions at 1200 MeV. Data from Ref. [67]. Same convention as in Fig. 4 for the display of the spectra.

in the IAEA Intercomparison report [17]. See also Ref. [73], which contains results concerning excitation functions for production of He and H isotopes, using basically INCL4.5 + ABLA. We just display here some typical cases.

We first present results for $p + {}^{197}$Au collisions at 1200 MeV in Fig. 7. Globally, the agreement is fairly good, except for high-energy deuterons at large angles. We recall that at this incident energy [15], alpha particles are predominantly produced in the evaporation stage, ^{3}He are dominantly produced in the cascade stage, deuterons and tritons are produced in both stages, but definitely more in the cascade, as indicated in Table III (see also Ref. [73] for a discussion of these dominances and of their energy dependencies). The impressive agreement between calculations and data for α production is due to both INCL4.6 and ABLA07 models (evaporation yield is determined by the excitation energy left after the cascade). On the other hand the good description of the high-energy tails of all particle spectra is solely due to our cascade model. There is no practical difference between the predictions of INCL4.6

TABLE III. Average multiplicity of clusters produced in cascade and in evaporation stages for two systems, as given by the INCL4.6-ABLA07 model.

Cluster	p (1.2 GeV) + ^{197}Au		p (63 MeV) + ^{208}Pb	
	Casc.	Evap.	Casc.	Evap.
d	0.505	0.166	0.0335	0.00035
t	0.124	0.081	0.0102	0.00011
^{3}He	0.046	0.0067	0.00147	0.0
^{4}He	0.167	0.352	0.0141	0.0136

and those of INCL4.5. A comparison with INCL4.2 itself is impossible as cluster production is not included in this model. However, a similar cluster-production model (up to alpha particles) was implemented in the intermediate version [15], referred to later as INCL4.2 with clusters. The predictions of the latter are really satisfactory in the energy range (600 to 2500 MeV), in which it has been tested [15], except for high-energy α production, whose yield is underestimated by this intermediate version. Compared to INCL4.2 with clusters, INCL4.6 is significantly better on this latter point but the most important improvement regards production at low incident energy and production of heavier clusters (see Sec. III C5 below).

Results for a slightly different system ($p + {}^{208}$Pb) at low energy are displayed in Fig. 8. At such an incident energy, the average excitation energy of the remnant is very small, evaporation of charged particles is strongly hindered and lcps, even α particles, are predominantly produced in the cascade stage, as illustrated in Table III. So the comparison with the data of Ref. [61] offers a severe test of INCL4.6 and especially of the cluster-emission module. It can be said that, on average, the model captures the magnitude and shape of the spectra fairly well, although the agreement is not as good as at high energy. Of course, partial deficiencies can be seen. For d, t, and ^{3}He emission, cross sections are overestimated above the expected value of the Coulomb barrier ($\sim$13 MeV for unit charge particles) and underestimated at energies close to the incident energy and small angles. The importance of this last deficiency can hardly be assessed, since this part of the particle spectra comes partly from coherent processes, which are outside the scope of the cascade simulations. Finally, for α emission, the height of the Coulomb barrier used in the cascade ($\sim$26 MeV) is definitely too large. It is larger than the Coulomb-barrier height used in the ABLA07 version, which is around 15 MeV. The effect of this barrier is clearly seen in the α energy spectra shown in Fig. 8 because the evaporation of α particles, although not important, is not negligible. These considerations explain the presence of a dip in the spectra around 23 MeV. Such a dip is not present or not visible in the spectra of the other light clusters.

We mention that the kind of agreement achieved in Fig. 8 crucially relies on criterion (6). If this condition is removed, the yield of low-energy clusters is badly overestimated.

We cannot introduce more figures here, due to lack of space, but we can say that roughly the same kind of agreement with experimental data is also reached for target nuclei as light as ^{27}Al.
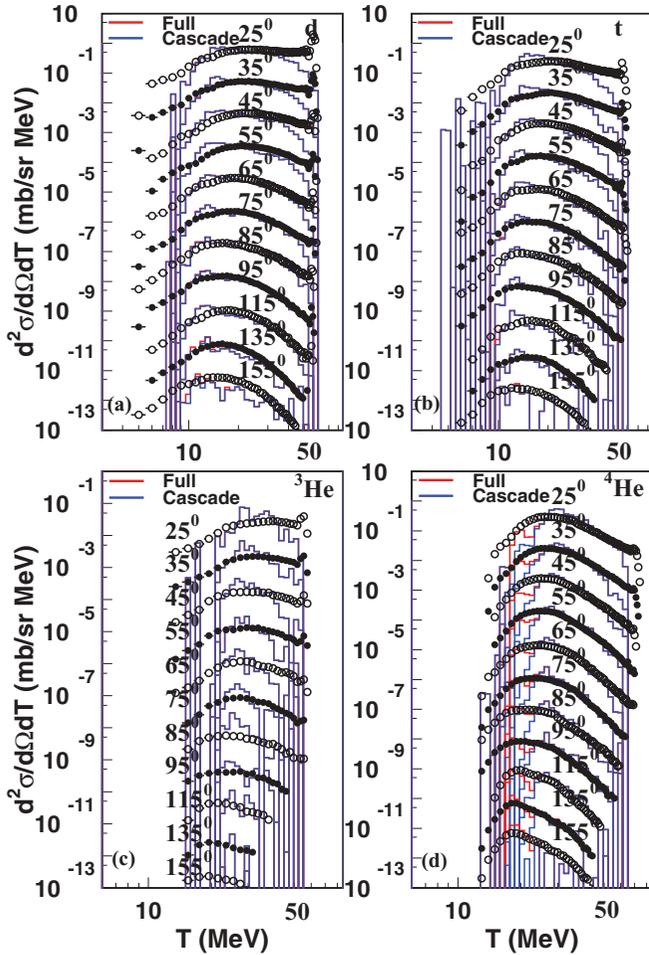
FIG. 8. (Color online) Comparison of INCL4.6 predictions (red) to the experimental data (symbols) for the double-differential cross sections for deuteron [panel (a)], triton [panel (b)], ^{3}He [panel (c)], and ^{4}He [panel (d)] production in $p + ^{208}$Pb collisions at 63 MeV. The blue curves give the cascade contribution (only the blue curve is visible when the blue and red results are identical). Data from Ref. [61]. Same convention as in Fig. 4 for the display of the spectra.

5. Heavier-cluster energy spectra

This paragraph refers to emission of clusters heavier than alpha particles. The separation between light clusters ($A_{cl} \leqslant 4$) and heavier clusters may appear arbitrary. However, if the production of light clusters by a sort of coalescence mechanism is more and more accepted, the one of heavier clusters by the same mechanism may appear doubtful. Here we want to point out some illustrative results obtained with the INCL4.6 + ABLA07 model, including the dynamical coalescence model described in Sec. II C2. We show in Fig. 9 the double-differential production cross sections of ^{6}He and ^{7}Be clusters in $p + ^{197}$Au collisions at 1.2 GeV. One can see that our model reproduces rather well the magnitude of the cross sections and the shape of the spectra. Notice that this is not an obvious result since, for instance, the ^{6}He cross section is almost an order of magnitude larger than the ^{7}Be cross section. Figure 9 also shows that these ions are predominantly produced in the cascade, at least for kinetic energies larger
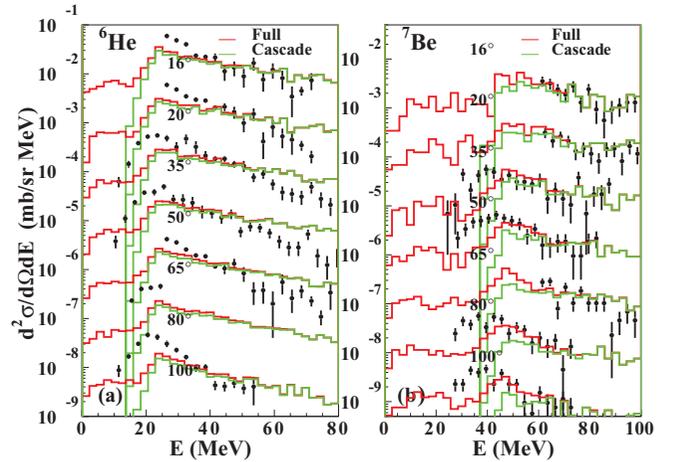
FIG. 9. (Color online) Double-differential cross section for ^{6}He [panel (a)] and ^{7}Be [panel (b)] cluster production in $p + ^{197}$Au collisions at 1200 MeV. The predictions of INCL4.6 + ABLA07 (red histograms) are compared with the experimental data of Ref. [72] (black points) at different angles, indicated in the panels. The green histograms indicate the cascade component. Same convention as in Fig. 4 for the display of the spectra.

than ~20 MeV for ^{6}He and ~30 MeV for ^{7}Be. The situation is different for the production of ^{6}Li and ^{7}Li, shown in Fig. 10. These clusters are predominantly produced in the evaporation, but the large-energy part of the spectra, say above 50 MeV, is explained by the production in the cascade. Notice that these results are less satisfactory than those displayed in Fig. 9, since our predictions seem systematically too low around 50 to 60 MeV. We calculated production cross sections for other targets and other energies. Because of lack of space, results will not be given here and will be described in a future presentation. Some partial results are contained in Ref. [33]. Let us just mention here that our model yields similar results as those displayed in Fig. 9. However, at low incident energy (~200 MeV [74] or less), most of the energy spectra are too hard [75]. This matter is in progress. Nevertheless, our present results are rather unique in explaining the production
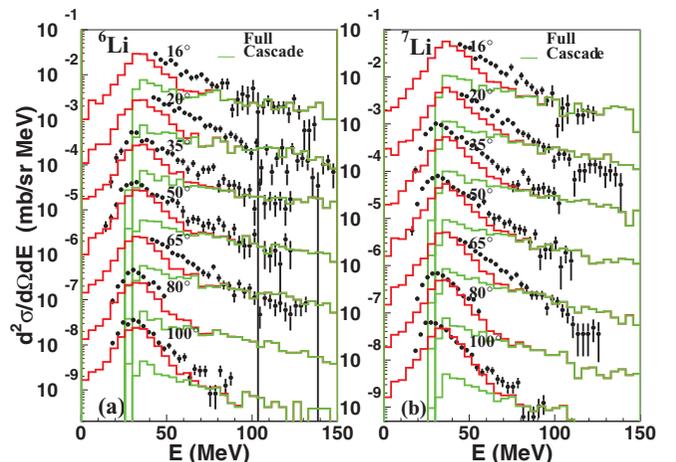
FIG. 10. (Color online) Same as Fig. 9 for ^{6}Li and ^{7}Li production cross sections.
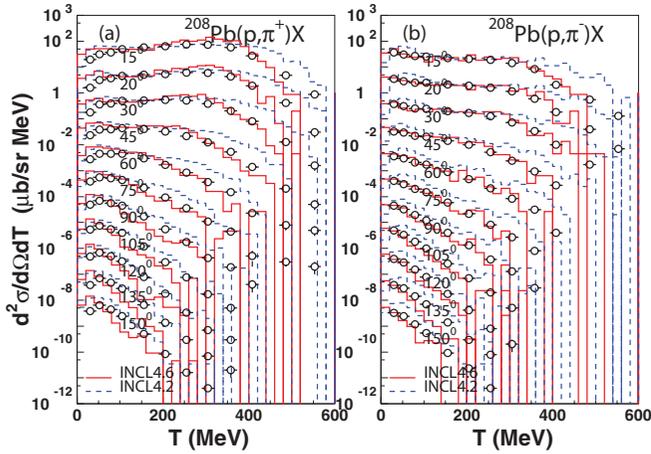
FIG. 11. (Color online) Comparison of INCL4.2 (dashed blue lines) and INCL4.6 (red lines) predictions with experimental data for inclusive π^+ [panel (a)] and π^- [panel (b)] double-differential cross sections in $p + {}^{208}\text{Pb}$ collisions at 730 MeV. Data are from Ref. [76]. Same convention as in Fig. 4 for the display of the spectra.

of heavy clusters by a dynamic coalescence model. At least they give credit to the plausibility of this mechanism, even if the details may not totally correspond to our coalescence model of Sec. II C 2.

6. Pion energy spectra

We will not expand very much on this point, since it is of small direct importance for applications (note, however, that pion production involves Δ excitation, which influences sizably the energy flow at high incident energy). We present some results in Fig. 11. It can be seen that INCL4.6 describes the data quite well, especially for negative-pion production. These results present a real improvement compared to INCL4.2. The respective magnitudes of the π^+ and π^- cross sections are well reproduced, indicating the correct isospin dependence of the elementary cross sections. The differences at low energy are coming rather from the introduction of the pion potential well and the Coulomb barrier effects. Whereas the predictions are correct for π^-, an overprediction of the π^+ cross sections appears slightly above the Coulomb barrier. This shortcoming was already present in INCL4.2, but it is now significantly reduced.

D. Residue production

1. Introduction

Residue production properties are determined by both the cascade and the evaporation stages, whose respective influences cannot often be easily disentangled. Furthermore, the ABLA model which has been used with INCL4.2 is not the same as the (new) ABLA07 model which has been used with INCL4.6 (and INCL4.5). This complicates the analysis. Therefore we will limit ourselves to a few significant results which may enlighten the merits and deficiencies of INCL4.6. More information can be found in Refs. [17–19].
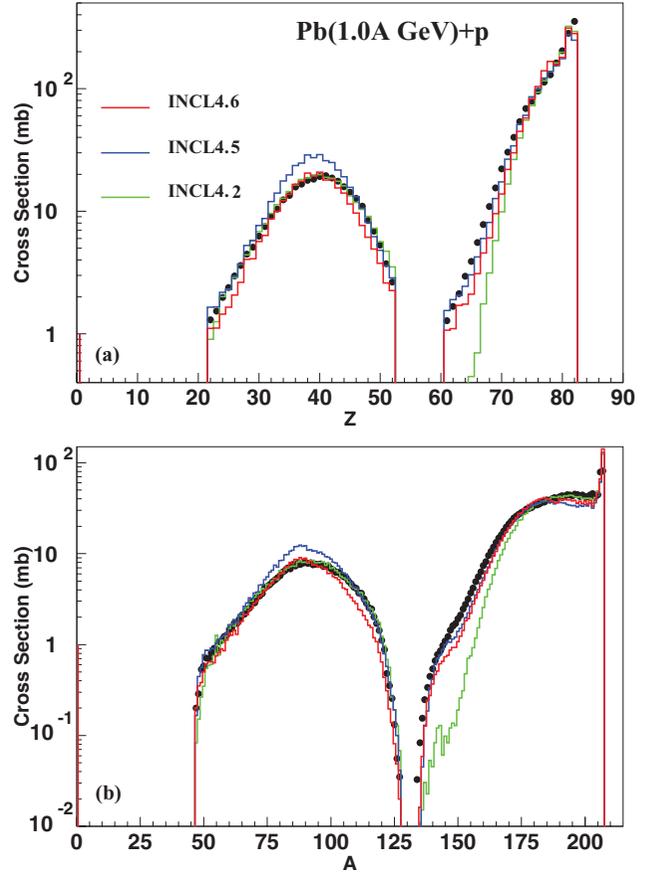
FIG. 12. (Color online) Comparison of INCL4.2 (green lines), INCL4.5 (blue lines), and INCL4.6 (red lines) predictions with experimental data for residue charge [panel (a)] and mass [panel (b)] spectra in $p + {}^{208}\text{Pb}$ collisions at 1 GeV. Data are from Ref. [77].

2. Residue mass and charge spectra

We present in Fig. 12 the predictions of INCL4.2 and INCL4.6 for mass spectra with the experimental data concerning the illustrative case of $p + {}^{208}\text{Pb}$ at 1 GeV. The theoretical results have been improved on the low-mass side of the so-called evaporation residue peak and have been deteriorated in the $A = 180$ to 200 region and to a lesser extent in the fission peak.

We now try, for this typical case, to disentangle the changes brought by the modifications of the our cascade model from those introduced by the changes in the ABLA model. In the changes from INCL4.2 and INCL4.6, listed in Secs. II C and II D,

TABLE IV. Average value of mass number A, charge number Z, excitation energy E^* (in MeV), and angular momentum J (in units of $\hbar$) of the remnant in $p + {}^{208}\text{Pb}$ collisions at 1 GeV, as calculated by different versions of INCL.

INCL version	$\langle A \rangle$	$\langle Z \rangle$	$\langle E^* \rangle$	$\langle J \rangle$
INCL4.2 without clusters	202.73	80.51	135.9	16.81
INCL4.2 with clusters	201.92	80.13	137.5	
INCL4.5	203.0	80.4	166.4	16.44
INCL4.6	202.7	80.4	157.5	16.04
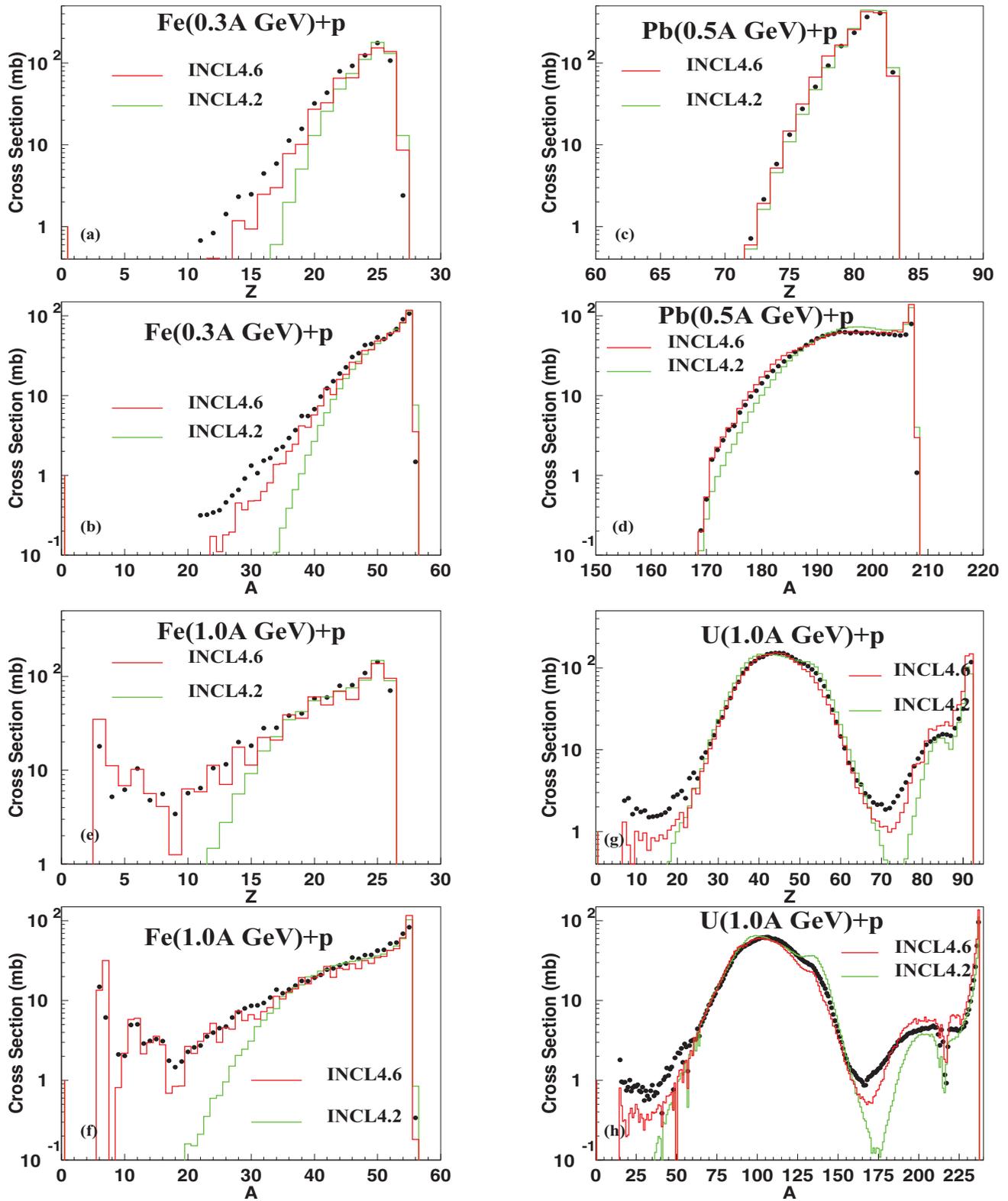
FIG. 13. (Color online) Comparison of INCL4.2-ABLA (green lines) and INCL4.6-ABLA07 (red lines) predictions with experimental data for residue charge [panels (a), (c), (e), and (g)] and mass [panels (b), (d), (f), and (h)] spectra in $p + {}^{56}\text{Fe}$ at 300 MeV (upper-left quarter), $p + {}^{208}\text{Pb}$ at 500 MeV (upper-right quarter), $p + {}^{56}\text{Fe}$ at 1 GeV (lower-left quarter) and $p + {}^{238}\text{U}$ at 1 GeV (lower-right quarter), respectively. Data are from Refs. [79–85].
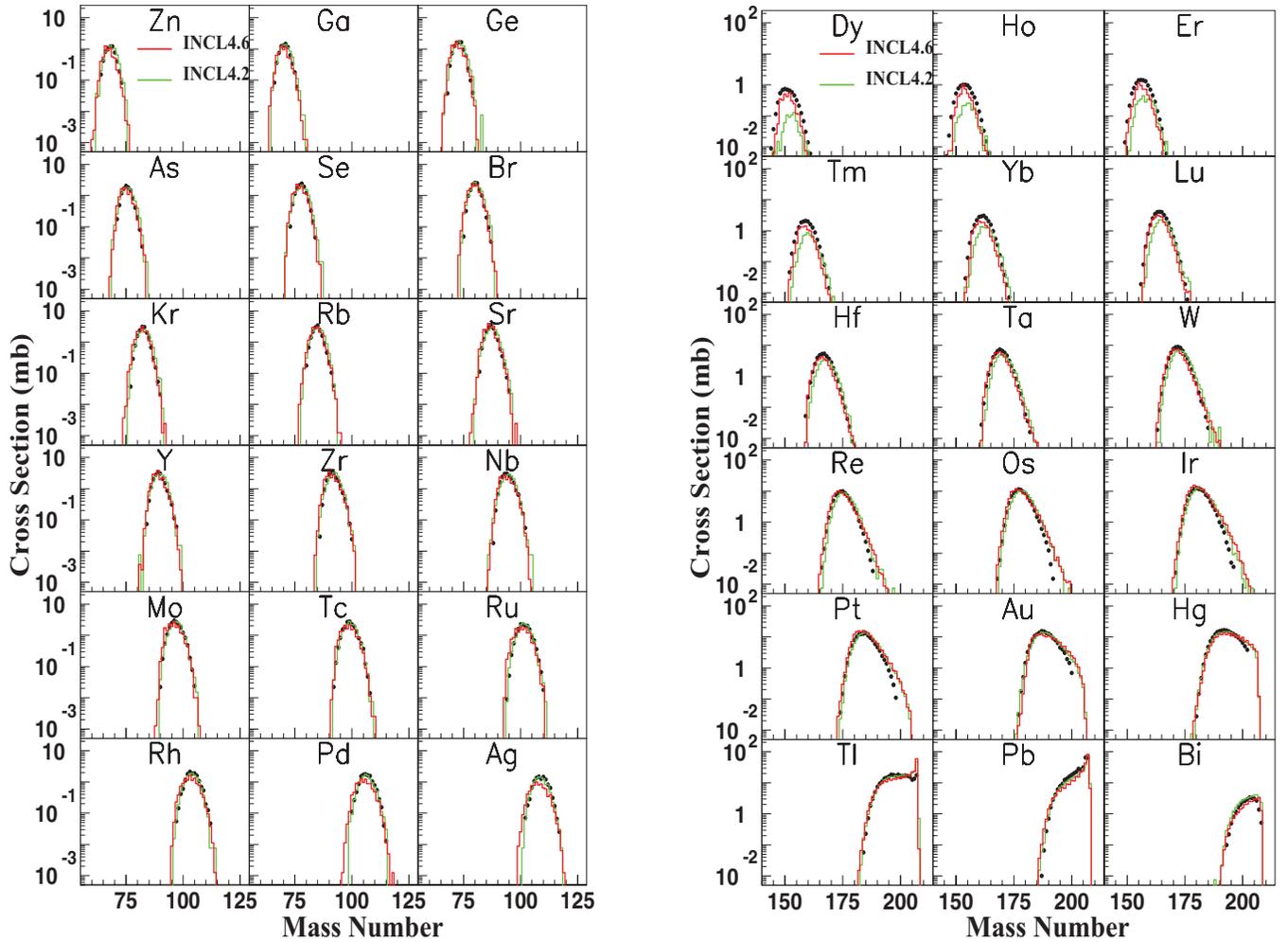
FIG. 14. (Color online) Comparison of INCL4.2-ABLA (green lines) and INCL4.6-ABLA07 (red lines) predictions with experimental data, for so-called isotropic distributions in $p + {}^{208}$Pb collisions at 1 GeV. The left panel shows typical isotopes produced as fission fragments and the right panel shows typical evaporation residues. Data are from Ref. [77].

the ones that are the most relevant for the residue mass spectrum are the introduction of cluster emission and the back-to-spectators trick. They, of course, influence the mass, charge, excitation energy, and angular momentum of the remnants. To enlighten the discussion we give in Table IV, the average value of these quantities for the different versions of INCL. It can be seen that the introduction of cluster production slightly increases the average excitation energy and slightly decreases the average mass of the remnant. The back-to-spectators trick produces, as expected, a strong increase of $\langle E^* \rangle$ (even when this trick is "corrected" as in INCL4.6) and a slight increase of the average mass of the remnant. The increase of the excitation energy is likely at the origin of the better description of the mass spectrum at the low-mass end of the so-called evaporation peak. It is presumably responsible for the underevaluation of the cross section in the $A = 185$ to 200 region. However, the competition with fission may play a role as well in this region. The various changes introduced in the ABLA code [53,78] precludes a detailed determination of the respective influences of the model. Roughly speaking, one can say that the fission

probability, for excitation energy and fissility parameter typical of the system above, has decreased from ABLA to ABLA07. Further small changes in ABLA07 when coupled to INCL4.5 and INCL4.6 have increased the fission probability. Figure 12 seems to indicate that the fission probability is probably rather satisfactory and that the remaining lack of cross section in the $A = 185$ to 200 region is due to other features.

For the sake of illustration, we give the charge and mass spectra for other systems in Fig. 13. One can see that the predictions of the INCL4.6-ABLA07 model are in good global agreement with the experimental data. We comment on the remaining discrepancies. The so-called deep spallation products are underestimated in $p + {}^{56}$Fe at 300 MeV. This is also the case for the $A \sim 15$ residues in the $p + {}^{56}$Fe at 1 GeV and for the $A \sim 160$ to 170 residues in the $p + {}^{238}$U system at 1 GeV. This might indicate an underestimation of the frequency of high-excitation events. But this may as well indicate an underevaluation of the emission of the large clusters in the de-excitation. At least this seems to be corroborated, for the $p + {}^{238}$U system, by the underpredicted yield of the $A \sim 20$

to 40 residues, since this kind of residues is expected to be produced by evaporation (beyond multifragmentation, which very likely is not operative in this system [86]).

We have to underline the almost perfect description of the mass spectrum in $p + {}^{208}\text{Pb}$ collisions at 500 MeV. Only the $A = 207$ yield is overestimated.

Let us comment on the fission fragment distribution in the $p + {}^{238}\text{U}$ system. Although the magnitude and the width of the fission peak are well reproduced, some features are not satisfactory. On the one hand, the shape of the fission peak is not so well accounted for, probably signaling inappropriate shell effects. On the other hand, the plateau in the $A = 200$ to 225 region is somehow overestimated, pointing probably to an imperfect evaporation-fission competition at large excitation energy.[5]

Finally, let us notice that odd-even effects are too large in $p + {}^{56}\text{Fe}$, presumably due to a too-large pairing used in ABLA07.

As for the isotopic distributions, we restrict ourselves to show our results for the illustrative case of $p + {}^{208}\text{Pb}$ at 1 GeV in Fig. 14. The shapes of these distributions for fission products are very well reproduced by both INCL4.2-ABLA and INCL4.6-ABLA07 models, with a slightly better performance for the first model. The isotopic distributions for evaporation residues (right panel) are well reproduced by the INCL4.2-ABLA model, except for the overall yield for the lightest ones. On the contrary, the INCL4.6-ABLA07 model does not suffer from this disease, but some deficiencies appear in the shapes of the distributions for the residues close to the target: the Pb isotopic distribution is underestimated around $A = 200$, the Os to Hg ($Z = Z_T - 6$ to $Z = Z_T - 2$) distributions are overestimated on the neutron-rich side and the ${}^{207}\text{Tl}$ ($Z = Z_T - 1$, $A = A_T - 1$) production cross section is sizably overestimated (this was also the case in INCL4.2). These deficiencies seem to come from a too-low excitation energy for those remnants that are located on the neutron-rich border of the so-called evaporation corridor (i.e., the region of the (N, Z) plane populated by the residues), close to the target. We have not been able to convincingly relate these deficiencies to the change of a specific parameter or to the removal of a specific hypothesis. Let us notice that the INCL4.6-ABLA07 model reproduces rather nicely the distribution for the Bi isotopes ($Z = Z_T + 1$) produced through (p, xn) reactions.

Similar deficiencies occur in the other systems referenced in Fig. 13 for isotopes close to the target, although these deficiencies have a smaller amplitudes in the $p + {}^{56}\text{Fe}$ system at 1 GeV and they are almost vanishing in the same system at 300 MeV.

3. Residue recoil velocity

Longitudinal recoil velocity measurements have been performed in inverse kinematics experiments carried on at GSI. We present typical results in Fig. 15, along with our predictions, for proton-induced reactions for ${}^{56}\text{Fe}$ and ${}^{208}\text{Pb}$
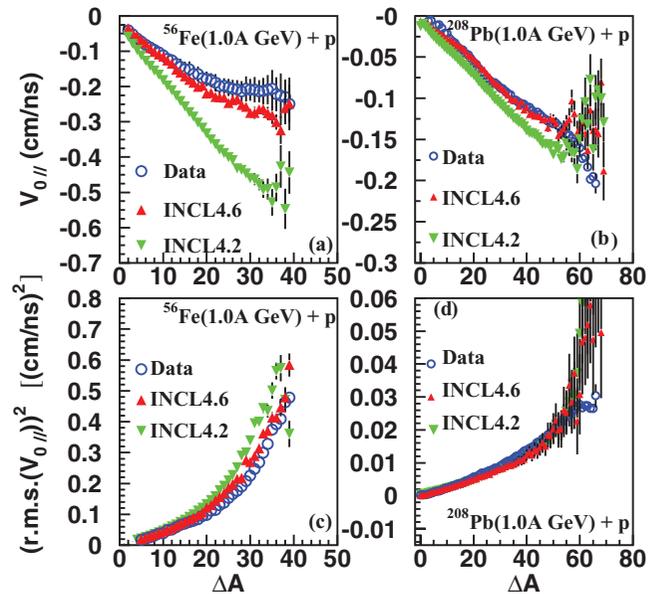
FIG. 15. (Color online) Recoil velocity of the residues. Comparison of INCL4.2-ABLA (green symbols) and INCL4.6-ABLA07 (red symbols) predictions with experimental data (blue circles), for the average value [panel (a)] and for the variance [panel (c)] of the velocity distributions, as functions of the mass loss ΔA (equal to the target mass number minus the residue mass number), for $p + {}^{56}\text{Fe}$ collisions at 1 GeV. Panels (b) and (d) refer to $p + {}^{208}\text{Pb}$ collisions at the same energy. Data are from Refs. [77,79].

at 1 GeV. The predictions of INCL4.6-ABLA07 for the average values of the longitudinal recoil velocity of the residues agree quite well with the data for mass losses $\Delta A = A_T - A$ up to $\sim$50 for $p + {}^{208}\text{Pb}$ and to $\sim$15 for $p + {}^{56}\text{Fe}$ (roughly one quarter of the target mass number for both systems). For the former system, the apparent lack of agreement for $\Delta A \gtrsim 50$ is presumably (or at least partly) due to large fluctuations in the calculation arising from very small cross sections (see Fig. 12). For the other system, the production cross sections remain sizable for very large mass losses (relative to the target mass), and Fig. 15 indicates that our predictions start to depart from experiment when mass loss gets larger than 20.

Panels (c) and (d) of Fig. 15 indicate that the predictions of the INCL4.6-ABLA07 model concerning the fluctuations are in remarkable agreement with the experimental values, even for larger intervals of mass loss (predictions of the previous INCL4.2-ABLA model are also remarkably close), for both systems.

These results provide a severe test for the cascade model. The average velocities are largely determined by the cascade process and the subsequent evaporation, being basically isotropic (in the remnant frame), does not bring a significant contribution. This is also true, to a lesser extent, for the rms fluctuations of the longitudinal velocity, except when evaporated particles are more numerous than the cascade ejectiles (i.e., when $\Delta A \gtrsim 40$ for $p + {}^{208}\text{Pb}$ and to $\sim$15 for $p + {}^{56}\text{Fe}$.

Our INCL4.6 cascade model is thus very successful in describing these observables and in picking up the basic

---

[5]The dip around $A = 214$ is due to very-short-lived α emitters which escape detection.
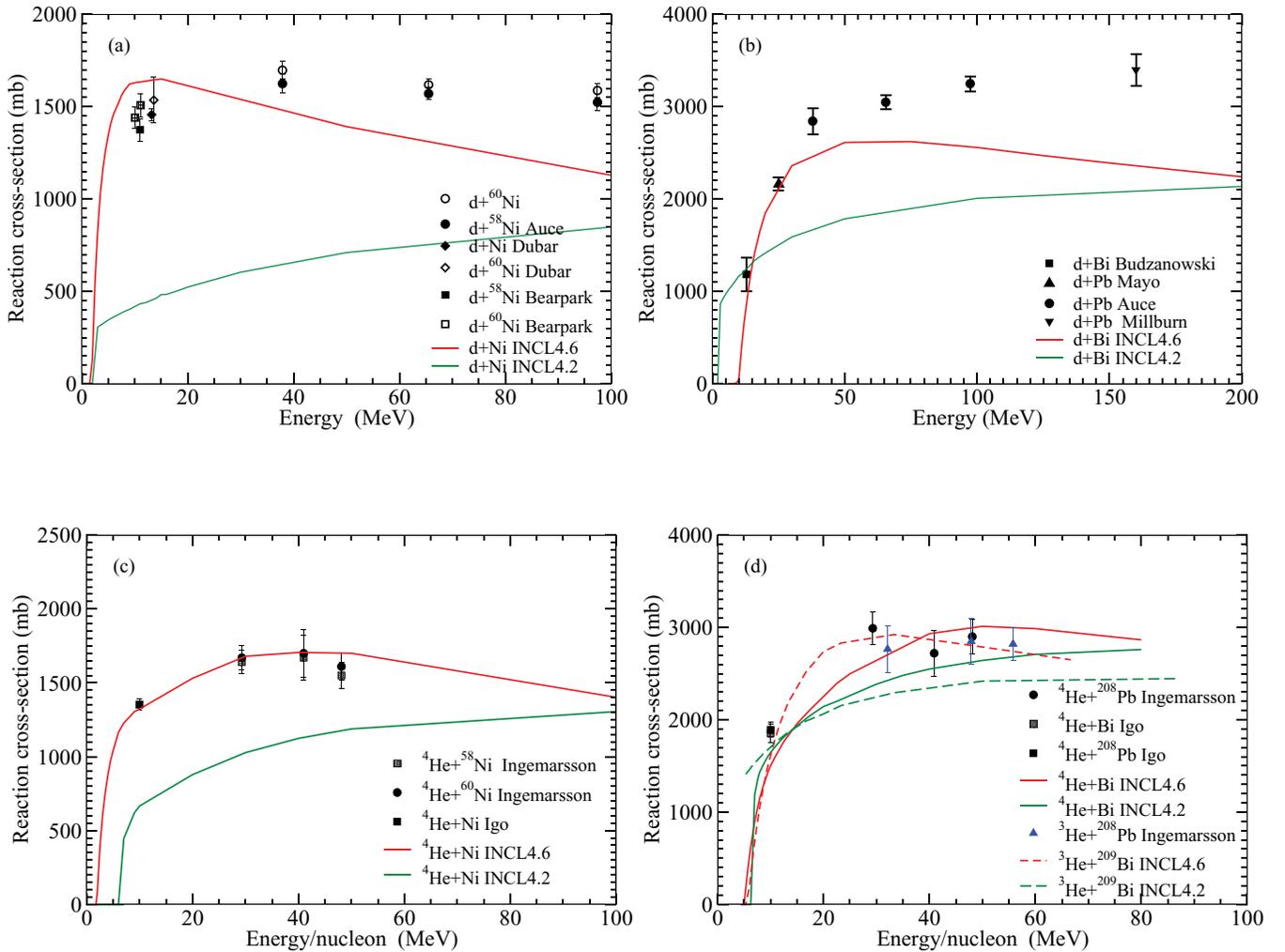
FIG. 16. (Color online) Total reaction cross sections (in mb) for deuterons on Ni and Fe target nuclei [panel (a)] and on Pb and Bi targets [panel (b)] as functions of the incident kinetic energy. The predictions of the INCL4.2 (INCL4.6) model are given by the green (red) curves. Panels (c) and (d) show the same comparison for α or ^{3}He incident particles, with cross sections plotted as functions of the incident kinetic energy per nucleon (for ^{3}He and ^{4}He). Same meaning for the full green and red curves. In panel (d), the dotted curves refer to ^{3}He reaction cross sections. Data are taken from Refs. [90–99]. The correspondence of the data with the particular reacting systems is given in the panels.

features of the generation of the recoil. It becomes less good in describing the average velocities for large mass loss in $p + {}^{56}$Fe at 1 GeV presumably because this system is characterized by a strong depletion of the target, for which models like INC are becoming less suitable.

For relatively small mass losses ($\lesssim 15$ for Fe and $\lesssim 30$ for Pb), the contribution of evaporation to rms fluctuations remains small. In these conditions, which allow a test of the cascade alone, the average value of the longitudinal recoil velocity and its variance is remarkably linear in the mass-loss variable, both in INCL4.6 and in experiment. As discussed in Ref. [11], this is an indication of the recoil resulting from a diffusion process, arguably due to independent successive NN collisions. The quality of the predictions of our cascade model appears as a strong support of its basic premises. We will not elaborate on this point here. We will instead discuss a little bit the difference between the results obtained by INCL4.6 and INCL4.2. Definitely, the predictions of the former are

an improvement over those of the latter for the average velocity, whereas the differences are rather minute for the rms. fluctuation. For the average velocity, we checked that more than half of the difference for the Pb case, and almost the whole difference for the Fe case, seems to come from the introduction of the emission of clusters in the cascade. In some sense, this emission allows a larger mass loss (in the cascade) without changing very much the pattern of the collisions for energetic participants (which are supposed to contribute the most to the recoil); that is, without changing the recoil velocity and the excitation energy. For a given recoil velocity, this leads to a corresponding increased mass loss. In simple terms, this pushes the curve for the average velocity in Fig. 15 toward the right of the figure. We could not isolate clearly the cause of the remaining difference. Presumably it is due to the introduction of forbidding collisions below the Fermi level (item 3.B of Sec. II C) and to the introduction of the back-to-spectators trick (item 1 of Sec. II D). Neither affect

very much the collisions involving energetic participants, but slightly increase the excitation energy. Thus, they increase the mass loss for a given recoil velocity, pushing also the recoil velocity curve of INCL4.2 toward the right.

For completeness, we mention that we made the same calculation for $p + {}^{56}$Fe collisions at 500 MeV (not shown here). The results are slightly better than at 1 GeV.

IV. RESULTS FOR CLUSTER-INDUCED REACTIONS

A. Introduction

As we said in the introduction, INCL4.2 can accommodate light clusters as projectiles, considering them as collections of on-shell nucleons with Fermi motion and a collective velocity adjusted in such a way that the total energy of the projectile nucleons (in the target frame) is equal to the nominal projectile incident energy. This method is justified at high incident energy (where the difference between the adjusted velocity and the nominal velocity is small anyway). Indeed, in Refs. [11,34], good results were obtained for deuteron-induced collisions around 1 GeV and departures from the simple additivity of a proton and a neutron cascades were illustrated. Satisfactory results were also obtained for other clusters in Refs. [39,40]. At low energy, this simple method cannot be accurate. Even more, the adjusted velocity cannot be defined for incident kinetic energy lower than the binding energy of the incident cluster. To cure this situation, we have introduced the method described in Sec. II D4. Our interest is mainly motivated by applications, in particular to accelerator-driven systems and spallation targets, as quoted in the introduction. As an example, astatine isotopes can be produced in Pb-Bi thick targets through, for instance, (α, xn) reactions induced by secondary α particles [87–89]. Following this motivation, we will mainly devote our attention here to the residue-production cross sections.

B. Total reaction cross sections

A set of total reaction cross sections is given in Fig. 16. Since this quantity is slowly varying with target mass and even with projectile mass, for the same velocity, we mix data for neighboring target nuclei. Although the experimental data are rather scarce, one can see that our model roughly picks up the basic properties of the energy dependence of the reaction cross sections; namely, a rapid rise at low energy followed by a slowly varying plateau. The magnitude of the plateau value is particularly well reproduced for incident α particles. For the d-induced reactions, this plateau value is underestimated. This may be explained by the contribution of the Coulomb dissociation of the deuteron, which is not taken into account. Evaluations of this contribution performed in Refs. [34,100–104] point toward a sizable cross section, of the order of 100 to 300 mb for the d-Pb system. This contribution is expectedly smaller for d-Fe and somehow negligible for α-induced reactions because of the large binding energy and the compactness of this projectile. One may notice the spectacular improvement obtained by INCL4.6, especially for deuteron-nucleus reaction cross sections. Of course, this is

consistent with the better reproduction of the nucleon-nucleus cross section by INCL4.6 in comparison with INCL4.2, as discussed in Sec. III B, due itself to a better treatment of the first collision at low incident energy. The predictions of INCL4.2 are closer to those of INCL4.6 for α particles compared with deuterons because, for peripheral collisions, the probability of interaction increases with the number of nucleons of the projectile. Finally, the threshold behavior is different in INCL4.2 and INCL4.6: in the former, it is mainly dictated by the value of binding energy per nucleon of the projectile whereas, in the latter, it is mainly dominated by the introduction of the Coulomb deflection and of the fusion (compound nucleus) process.

Let us add a comment on the plateau values. First of all, the maximum of the cross section is loosely correlated with the maximum which occurs in the proton-nucleus cross sections for the same target at low energy (see Fig. 2). The value of the reaction cross section at the maximum for cluster-induced reactions is larger than the maximum value of the proton-nucleus cross section and reflects the size of the cluster, which allows interactions for larger impact parameters. Let us finally indicate that the slow decrease of the cross sections in Fig. 16 is presumably related to the decrease of the NN cross section in this energy range.
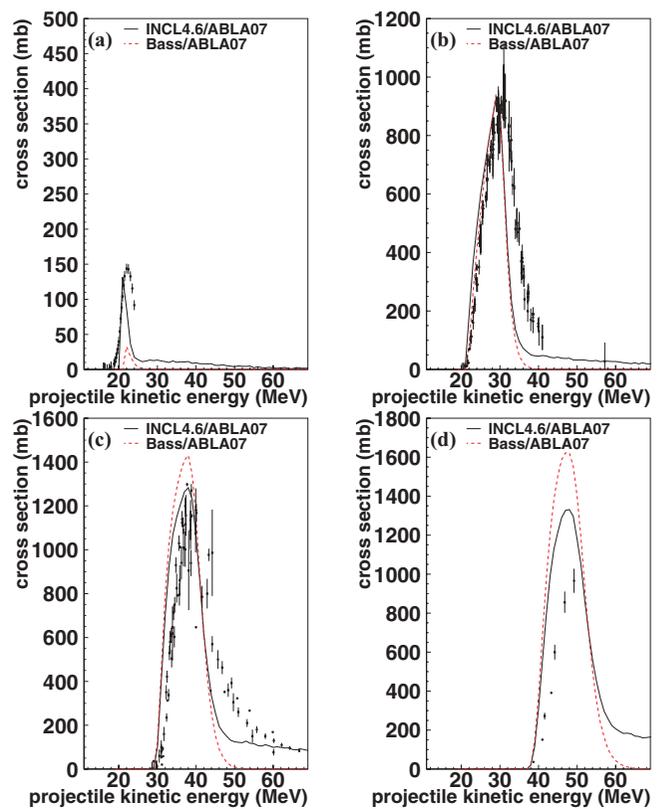
FIG. 17. (Color online) ^{209}Bi(α, xn) cross sections for $x = 1, 2, 3$, and 4, corresponding to panels (a)–(d), respectively, as functions of the incident α kinetic energy. The full black curves correspond to the predictions of the INCL4.6 + ABLA07 model. The dashed red lines represent the results using the Bass fusion model, followed by the ABLA07 model. Data are taken from Refs. [105–107].
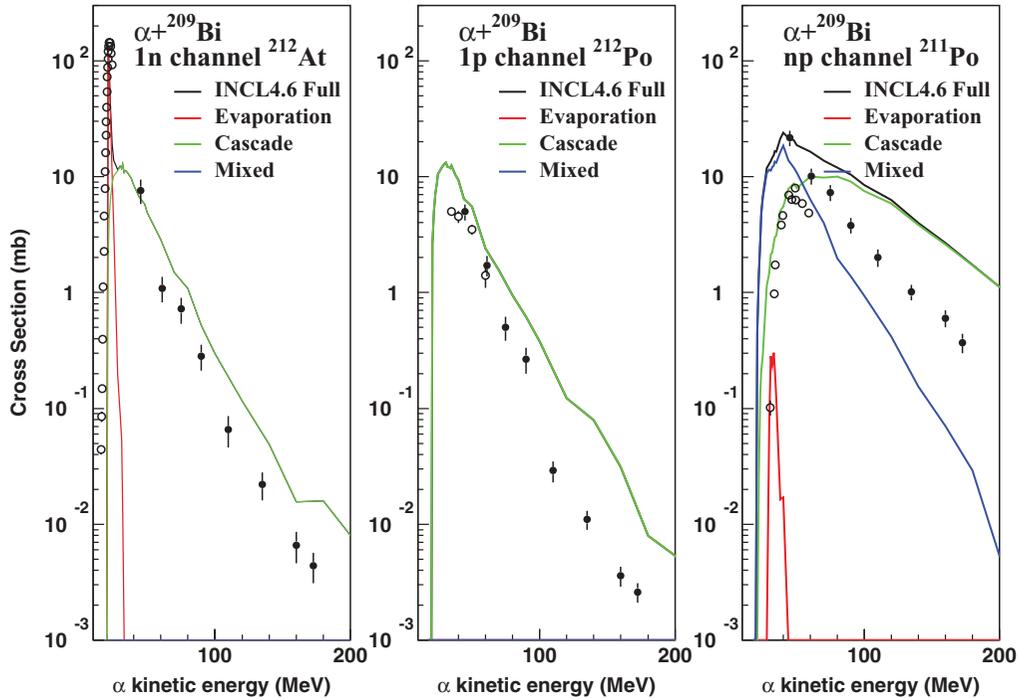
FIG. 18. (Color online) ^{209}Bi(α, n) (left), ^{209}Bi(α, p) (center), ^{209}Bi(α, np) (right) cross sections, as functions of the incident α kinetic energy. Each predicted cross section using the INCL4.6-ABLA07v5 model (black lines) is split into a cascade component (green lines), an evaporation component (red lines), and a mixed component (blue lines). See text for detail. The black lines give the sum of the three components and are visible when they are not identical to colored lines. Experimental data are taken from Refs. [105,108] for ^{209}Bi(α, n) and from Refs. [108,109] for the two other reactions.

C. Residue-production cross sections

As a first example of our results, we show in Fig. 17 the cross sections for the production of At isotopes through ^{209}Bi(α, xn) reactions. Globally, the shapes and the magnitudes of the peaks of the cross sections are satisfactorily reproduced. The correct position of the respective maxima indicates a good description of the competition between the successively opening channels in the evaporation. On the other hand, the good evaluation of their magnitudes indicates that the total reaction cross section is correctly given by the cascade model, as shown in Fig. 16. Figure 17 also shows the results of a calculation using the Bass fusion model [110], coupled to the ABLA07 de-excitation model. It can be seen that in these conditions, where fusion dominates, our model yields results which compare rather well with those of a very commonly used fusion model. It may be argued however that the Bass model is not really suitable for alpha particles.

A little bit more detail concerning the ^{209}Bi(α, n) reaction is given in the first panel of Fig. 18, where data from Ref. [108] at higher energy have been added to those of Ref. [105]. The high-incident-energy part of the excitation function is a good test of the cascade model. Indeed, we have divided the theoretical cross section in Fig. 18 into three components: the first one (in green) corresponding to events where the particles are ejected during the cascade stage,[6] the second one (in red) corresponding to events with particles emitted during

the de-excitation of the target remnant, and the last one (in blue) for events in which the emitted particles are coming partly from the cascade and partly from the evaporation stages. The red curves can be viewed as giving the complete fusion (plus evaporation) contribution whereas the two other curves can be interpreted as corresponding to incomplete fusion and/or pre-equilibrium processes. For the ^{209}Bi(α, n) reaction, the mixed (blue) component is identically vanishing, since a single neutron is emitted either in the evaporation of the fused system or in the cascade stage. From the first panel of Fig. 18, it can be seen that the cross section above $\sim$30 MeV incident energy is well described by our model. The emission of a single neutron is then entirely due to the cascade mechanism. The remnant (i.e., the compound nucleus) is then sufficiently excited to emit two neutrons, at least, with a large probability and thus does not significantly feed the 1n channel. The same is true for the ^{209}Bi(α, p) reaction (shown in the central panel of Fig. 18). In that case, the evaporation component is very much suppressed, even in the 20 to 30 MeV range, due to the Coulomb barrier. Finally, the third panel of Fig. 18 displays the situation for the ^{209}Bi(α, np) reaction. Here, above $\sim$70 MeV incident energy, the cross section is dominated by the emission of the neutron and the proton during the cascade stage. At lower incident kinetic energy, there is a very small component for the emission of the two nucleons in the evaporation stage, but at low incident kinetic energy the cross section is dominated by the mixed emission of the two particles.

Another example is provided by Fig. 19, which shows deuteron-induced reactions on ^{209}Bi. The shapes of the cross

---

[6]This includes the geometrical spectators.
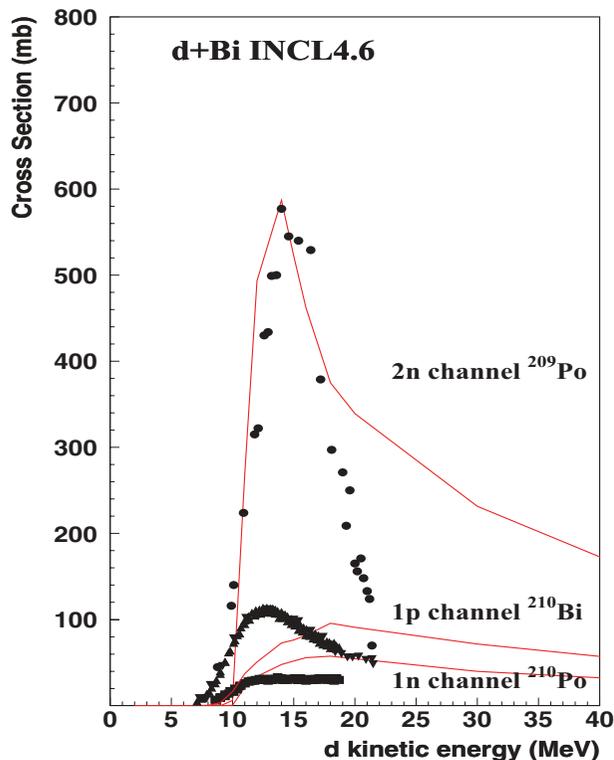
FIG. 19. (Color online) Deuteron-induced reactions on ^{209}Bi. The predictions of the INCL4.6-ABLA07 model (full red lines) are compared with experimental data (symbols) relative to ^{209}Bi(d, n) (squares), ^{209}Bi$(d, 2n)$ (full dots), and ^{209}Bi(d, p) (triangles) reactions. Cross sections are given as functions of the deuteron incident kinetic energy. Data from Refs. [98,111,112].

FIG. 20. (Color online) ^{181}Ta(α, xn) cross sections for $x = 1$ (blue), 2 (green), 3 (red), and 4 (black), respectively, as functions of the α incident kinetic energy. The full lines correspond to the predictions of the INCL4.6 + ABLA07 model. Data (symbols) are taken from Ref. [113]. The dashed line gives the theoretical total reaction cross section.

sections are globally reproduced fairly well, although some details are missed. The decrease of the $(d, 2n)$ cross section on the right of the peak is somehow too slow. The precise threshold behavior for (d, n) and (d, p) reactions is not exactly reproduced, in spite of the use of exact Q values. Actually, the theoretical (d, n) and (d, p) cross sections are roughly the same. However, the experimental (d, n) cross section is roughly four times smaller than the (d, p) cross section in the region of the maximum ($\sim$10 MeV). This discrepancy might be due to the Coulomb dissociation of the deuteron. We will discuss this point below, after the presentation of another case.

Results concerning another heavy target are reported in Figs. 20 and 21. The first one shows the various ^{181}Ta(α, xn) cross sections as functions of the α incident kinetic energy. One can see a remarkable agreement between the predictions of our model and the experimental data. We also notice that the sum of the (α, xn) cross sections nicely exhausts the total reaction cross section.

The splitting of each of the (α, xn) theoretical cross sections into three components as defined in Fig. 18 is displayed in Fig. 21. The bump of each cross section is mainly due to evaporation. For the (α, n) reaction, the decreasing part of the cross section above the bump is entirely due to cascade. There is, of course, no mixed component in this case. Starting from $(\alpha, 2n)$ and going to more and more emitted neutrons, the mixed component grows and become dominant above the

bump region. This simply means that when the incident energy starts to correspond to this region, the excitation energy of the compound system becomes sufficient to emit $x + 1$ neutrons with a high probability, the (α, xn) cross section is sizably reduced and the underlying reaction mechanism resembles more and more to the standard spallation reaction mechanism, involving a cascade stage, possibly resulting in incomplete fusion, and followed by a de-excitation stage, both stages emitting particles. It is remarkable that both the shape and the magnitude of the various bumps and the trend of decreasing part of the cross sections are well described by our model. This means that our model is catching the main features of the compound nucleus formation at low energy and its progressive change into a mechanism involving so-called pre-equilibrium features.

We show in Figs. 22 and 23 the results of our calculation for ^{3}He-induced reactions on ^{181}Ta. If the trends are correctly accounted for, the agreement is much less satisfactory than for the ^{181}Ta(α, xn) reactions. The cross sections for $x = 1$ and $x = 2$ are substantially overestimated, and the one for $x = 3$ is still too large by a factor of two.

The ^{181}Ta$(^3$He$, xn)$ cross sections are split in the various contributions in Fig. 23. Several features have to be noticed: there is no evaporation component for $x = 1$, and the mixed component increases very sharply from the very opening of the
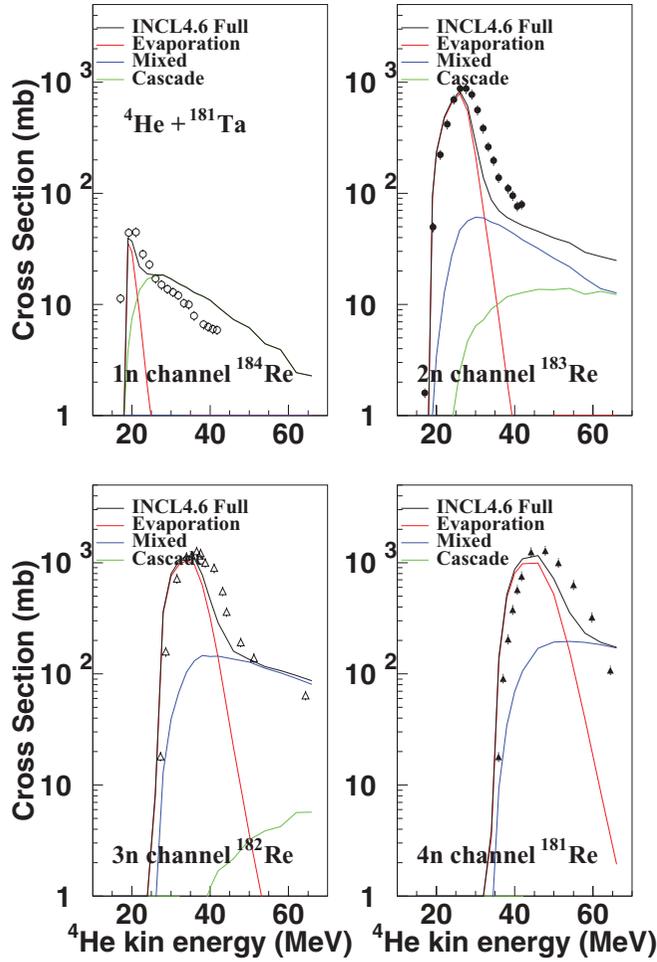
FIG. 21. (Color online) Splitting of the calculated ^{181}Ta(α, xn) cross sections (black lines) for $x = 1, 2, 3$, and 4, respectively, as functions of the α incident kinetic energy, into the various contributions: cascade (green), evaporation (red), and mixed (blue). The corresponding channel and residue are indicated on each panel. See text for detail. Data (symbols) are taken from Ref. [113].

FIG. 22. (Color online) Same as Fig. 20 for ^{181}Ta$(^3$He$, xn)$ reaction. Data (symbols) are taken from Ref. [113]. The dashed line gives the theoretical total reaction cross section.

cross section for $x = 2$ and $x = 3$. This component dominates for $x = 2$.

Before interpreting our results, we want to comment on the shapes of the experimental cross sections. For (α, xn) reactions, both for ^{181}Ta and ^{209}Bi, the cross sections show the typical pattern of raising and decreasing stages, replacing the $(x - 1)n$ cross section and then giving place to the $(x + 1)n$ cross section. This is due to the positive threshold values (the opposite of the Q value), increasing with x. For example, for the ^{209}Bi(α, xn) reactions, the threshold values are located at 15.56, 20.62, 28.43, and 35.61 MeV for $x = 1, 2, 3$, and 4, respectively. On the other hand, for the ^{181}Ta$(^3$He$, xn)$ reactions, the threshold values are -10.83, 3.88, 11.16, and 19.88 MeV. At the Coulomb barrier (roughly 15 MeV), the $(^3$He$, n)$, $(^3$He$, 2n)$, and $(^3$He$, 3n)$ channels are already open. That is why the cross sections, at least for $x = 1$ and 2, do not show a typical bump [as for ^{209}Bi(α, xn)], but rather a steady increase followed by a plateau. A compound nucleus formed at the Coulomb barrier has already an excitation energy of

25 MeV and has thus little chance to decay to the $1n$ exit channel and even to the $2n$ exit channel.

We now come back to our numerical results for ^{181}Ta$(^3$He$, xn)$. In accordance with the last remark, in our calculations (see Fig. 23), the $(^3$He$, n)$ channel is fed by the cascade only. According to Sec. II D4, the three nucleons of ^{3}He are lying above the Fermi energy, at the beginning of the reaction. Very likely, the neutron is emitted freely or quasifreely (after a soft collision for instance), and the two protons are kept inside the target with a small excitation energy, otherwise a neutron would be evaporated. The $(^3$He$, 2n)$ channel is largely dominated by a mixed emission: presumably, one of the neutrons is emitted (almost) freely, whereas the two protons initiate a cascade process leading to a remnant sufficiently excited to emit a neutron. The $(^3$He$, 3n)$ channel presumably corresponds to a transition toward a sequence of emissions by evaporation.

It seems to us that the overestimation in our model of the $(^3$He$, n)$, $(^3$He$, 2n)$ and perhaps $(^3$He$, 3n)$ cross sections indicates that the separation between compound nucleus and cascade regimes in our model, explained in Sec. II D4, is probably too crude, somehow underestimating the fusion and overestimating the cascade cross section.
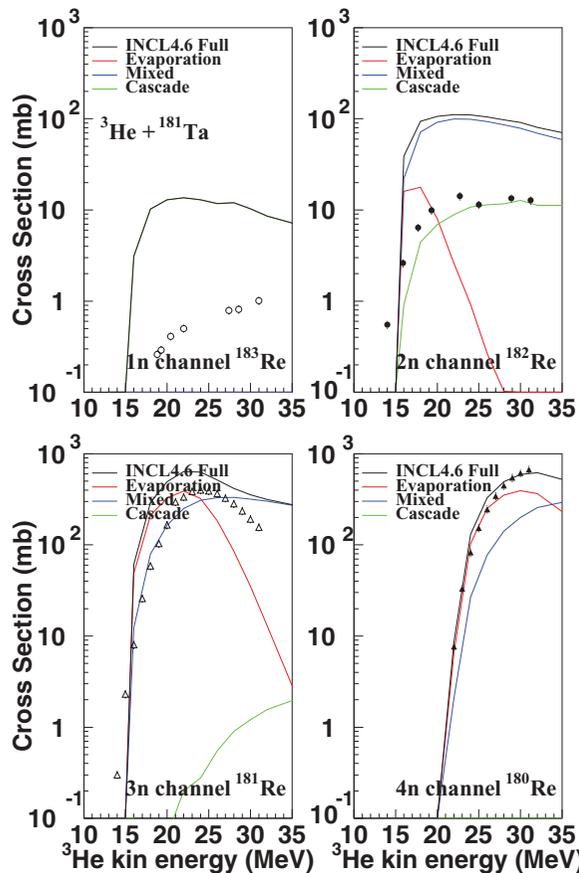
FIG. 23. (Color online) Same as Fig. 21 for ^{181}Ta(^{3}He, xn). For the $1n$ channel (upper-left panel), the green curve is identical to the black curve and is not displayed. Data (symbols) are taken from Ref. [113].

FIG. 24. (Color online) ^{56}Fe(α, n) (upper panel) and ^{60}Ni(α, n) (lower panel) cross sections. The full curves correspond to the predictions of the INCL4.6 + ABLA07 model and the symbols represent the experimental data. Data are from Refs. [117–121].

Another possible interpretation calls for the Coulomb dissociation of the projectile. One can imagine that, at low energy, below or slightly above the Coulomb barrier, the ^{3}He is dissociated, say in $d + p$, by the Coulomb field before it really hits the nucleus. If the deuteron escapes, the accompanying proton "sees" a Coulomb barrier which is twice as small as the one seen by the ^{3}He, but its kinetic energy is three times as small. The proton is thus repelled. This phenomena would shift a part of the (^{3}He, n) and (^{3}He, $2n$) cross section to other channels. An argument in favour of this interpretation, quoted in Ref. [113], comes from the fact that the sum of the experimental ^{181}Ta(^{3}He, xn) cross sections does not exhaust the total reaction cross section. This effect, based on Coulomb dissociation, is expected to be roughly controlled by a parameter that can be loosely defined as $\eta = (Zr)^2/B$, where Z, r, and B are the charge, the radius, and the binding energy of the cluster; that is, increasing with the electric polarizability of the projectile and inversely proportional to its "stability" [34,114–116]. On these grounds, one expects that the effects encountered for ^{3}He are largely reduced for α particles, as one may indeed observe above. However, the effect should be even more pronounced for deuterons. But this does not seem to be the case for the example of Fig. 19. Of course, the effect is expectedly reduced for light targets.

We now turn to illustrative results for light targets. Fig. 24 shows a comparison of our predictions with experiment concerning (α, n) reactions on ^{56}Fe and ^{60}Ni targets. The agreement for the ^{56}Fe(α, n) cross section is quite good. There are two sets of data points for the reaction ^{60}Ni(α, n). Our predictions are close to the data set of Ref. [117]. In addition, one can notice that our model is able to respect the difference between the cross sections for the two targets, which are in fact rather similar to each other. The reason is that our model properly takes account of the different Coulomb penetrablilities and, especially, of the real Q values. The latter are -5.053 and -7.938 MeV, for ^{56}Fe(α, n) and ^{60}Ni(α, n) reactions, respectively.

Another example is provided by Fig. 25. In contrast to the ^{3}He + ^{181}Ta case, illustrated in Fig. 23, the (^{3}He, n) and (^{3}He, $2n$) are now satisfactorily reproduced. Like for the previous case, these reaction channels are open at the Coulomb barrier, although not "wide" open. The thresholds for the two reactions are 3.41 and 5.07 MeV, respectively, and the Coulomb barrier lies around 8 MeV. The fact that we reproduce (^{3}He, n) and (^{3}He, $2n$) cross sections in this case and not in the ^{181}Ta case is not inconsistent with the explanation in terms of Coulomb dissociation of the ^{3}He in this latter case. Indeed, the probability of this dissociation is expected to be very small for a ^{59}Co target. Figure 25 also shows a (^{3}He, p) cross section for ^{63}Cu (in view of lacking data for
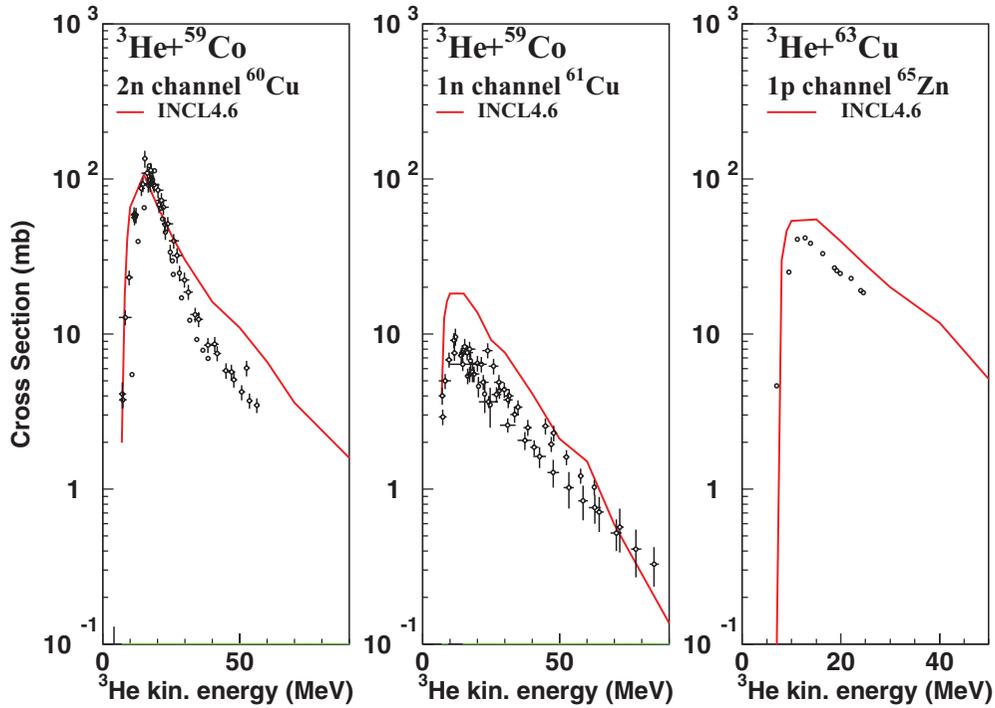
FIG. 25. (Color online) ^{59}Co(^{3}He, $2n$) (left), ^{59}Co(^{3}He, n) (center), ^{59}Co(^{3}He, p) cross sections, as functions of the ^{3}He incident kinetic energy. Comparison of the INCL4.6-ABLA07 predictions (red lines) with experimental data from Refs. [122–124].

^{59}Co a slightly different target is considered), for which our calculations reach a reasonable agreement with the data.

The last case refers to the ^{60}Ni(d, n) reaction, illustrated in Fig. 26. Although the opening of the channel is well described in our model, the cross section is noticeably underestimated, in similarity with the ^{209}Bi case (see Fig. 19). This observation may be consistent with the explanation in terms of the Coulomb dissociation. However, this effect should in principle be much smaller for ^{60}Ni, as stated above.

In summary, these examples and other similar examples that are not displayed here show that our model yields reasonable results for total reaction cross section and residue-production cross sections at low energy. This observation seems to indicate that the model efficiently describes the probability of forming a compound nucleus and the progressive appearance of pre-compound emission, despite the crudeness of its ingredients. The model can even describe threshold behavior satisfactorily, owing to the use of experimental Q values.

V. DISCUSSION AND CONCLUSION

We have presented here the updated and improved version (INCL4.6) of our standard INCL4.2 model. We recall that the philosophy at the origin of this latter model leads to include as much known microscopic physics as possible, without relying on parameters. Of course, this model relies on assumptions, as recalled in the introduction.

The extension of INCL4.2 has been done in two steps, giving birth to the INCL4.5 and INCL4.6 versions, described in Secs. II C and II D. Because the results obtained by INCL4.5

are available from the intercomparison organized by the IAEA [17], we emphasized here the results obtained by INCL4.6. We will also not compare with other INC models, since such a comparison has been done in Ref. [17], concerning the INC (or QMD) models described in Refs. [36,37,45–51,126,127]. It shows that our model, coupled to ABLA07, is one of the best combinations for the description of spallation reactions, at least for the set of data proposed in the intercomparison, basically nucleon-induced spallation reactions on key targets (mainly Fe and Pb) for incident energy spanning from ∼60 MeV to 3 GeV. See also Ref. [19] for a short analysis of the intercomparison and Ref. [128] for a similar intercomparison restricted to excitation functions of residue-production cross sections. The attention has here been focused more on observables which are accessible by INCL4.6 only or which have been ignored by the intercomparison, such as the recoil velocities and heavy-cluster production.

We first want to discuss the new features of our model. Part of the extension has been realized in the spirit of INCL4.2; namely, by introducing known and well-established phenomenology. This bears on the introduction of energy and isospin-dependent nucleon potentials, of pion potentials, of Coulomb deflection of charged particles, and of experimental Q values, as discussed in Sec. II D. The impact of these modifications on the results is globally modest. However, they are important for some peculiar features. This holds for (p, π) reactions [30] and threshold behavior of light cluster-induced reactions leading to the emission of a small number of nucleons (see Sec. IV C).

A second part of the extension that we want to single out consists of the introduction of the dynamical coalescence

FIG. 26. (Color online) ^{60}Ni(d, n) cross section, as a function of the deuteron incident kinetic energy. Comparison of the predictions of the INCL4.6 + ABLA07 model (red curve) with the experimental data of Ref. [125].

of ad hoc parameters or assumptions. The most intricate aspect of this remaining part of the extension is given by the new procedure for handling incident clusters. In INCL4.2, the incident cluster is considered as a collection of on-shell nucleons, gifted with Fermi motion and having a total energy equal to the incident total cluster energy. This approximation, which is pretty reasonable at high energy per nucleon of the incident cluster (compared to binding energy per nucleon and/or Fermi energy), is bound to fail at low energy. Therefore, in our opinion, it is necessary to account for the off-shell character of the nucleons while keeping total momentum and energy to their nominal values. Another necessary feature appears to be the almost unavoidable compound nucleus formation at very low energy, at least for sufficiently small impact parameters. In addition, incomplete fusion and/or soft excitations of the projectile should be made possible at grazing impact parameters. The last ingredient of a satisfactory reaction model should allow the progressive growth of the pre-equilibrium processes.

The surprising result of our study is that all these requirements can be met in a model using as basic quantities the four-momenta of all nucleons and leading to results in reasonable agreement with experiment. Even more, our model, whatever its ad hoc features, possesses the unique property of describing the gradual move from compound nucleus to pre-equilibrium processes with a unique set of assumptions. Usually, two distinct models are used, with sometimes an additional model to ponder the relative importance of compound nucleus and pre-equilibrium. Actually, we have achieved, in some sense, for cluster-induced reactions, the same objective as in our cascade model for nucleon-induced reactions; namely, describing absorption and so-called pre-equilibrium processes with the same cascade tools (propagation and binary collisions of individual nucleons). It should be stressed, however, that this objective has been attained on a rather empirical basis.

Let us now turn to a discussion of the predictive power of our new model. We first comment on nucleon, pion, and residue-production cross sections, either differential or global, for nucleon-induced reactions. These observables were already accessible by our previous model INCL4.2. We recall that some of the modifications included in INCL4.6 (even restricted to those which have an influence on the observables under consideration) may appear to have some ad hoc character, such as the treatment of soft collisions or the local E trick described in Sec. II C. As is often the case when ad hoc or empirical modifications are added to an already performing model, some of the results are improved and others are slightly worse than before. For instance, the cascade part of the neutron spectra are slightly worse with INCL4.6 than with INCL4.2, which gives an excellent reproduction of the data (see Fig. 4). On the other side, INCL4.6 generally gives more excitation energy than INCL4.2. As a consequence, the residue mass spectra have noticeably been improved (see Sec. III D2). A considerably important improvement brought by INCL4.6 concerns the prediction of the total reaction cross sections, which has also allowed an improvement of the results at low incident energy, well below 200 MeV, which is the limit of validity of the INC models that is usually quoted.

model for production of clusters during the cascade. It is based on the simple idea that an outgoing nucleon can carry along other nucleons which are close enough in phase space. We insist on the fact that this idea departs from usual coalescence models in two features: it deals with phase space and not momentum space, and it depends on the instantaneous distribution of the nucleons in the course of the cascade process and not on the final distribution. The importance of this difference is discussed in Ref. [15]. This model performs rather well with a single proximity parameter (valid for all light clusters) at high energy, say above 500 MeV. The model had to be refined at lower energy basically on two points: the proximity parameter had to vary moderately with the type of the cluster, and tangential emission of clusters had to suppressed. As far as the results are concerned, these modifications are a real advance, since emission of light clusters (up to α particles) are well reproduced by our model, down to 60 MeV incident energy. See Ref. [17] and Sec. III C. It is shown in Sec. III C5 that this model can be extended to emission of heavier clusters. We will comment on this point later on.

Finally, the remaining part of the extension is founded more on recipes, admittedly to remove discrepancies with experimental data, than on solidly established phenomenology or pieces of models. It is accompanied by the introduction

We now turn to the new potentialities of our improved model which, in our opinion, outpace the improvements mentioned above and others discussed in the paper. We will shortly comment on each of them.

(i) Our improved model allows for the production of clusters owing to the implementation of a dynamical coalescence model. We have presented here (and in Ref. [17]) results for double-differential production of light clusters, up to α particles, which are in rather good agreement with experimental data, for a wide range of incident energy and target mass. We have in addition showed that the production of heavier clusters with a kinetic energy larger than the typical evaporation energies can also be generated by the same mechanism. In our simulations, which require the production of all potential clusters, we are limited by computational time to $A \leqslant 8$ clusters. We have shown very promising results in Fig. 9, but not all cases show a similar agreement. Nevertheless, we are convinced that our implementation of the coalescence module is flexible and that a more involved search of the better parameters will give eventually an overall satisfying description.

(ii) In Sec. III D 3, devoted to the recoil of the residues, we show perhaps the nicest of our results. Recoil energies are small, but their knowledge is of uttermost importance for technological applications, since they determine the damage to materials under irradiation. We think it is an important result because the agreement with experiment is impressive, but also because the distribution of the recoil velocity shows the fingerprint of a diffusion process, which is in concordance with the description of the reaction process as a succession of independent binary collisions.

(iii) In Sec. IV, we set out our model for cluster-induced reactions. If at high incident energy the cluster can be viewed to first approximation as a collection of individual nucleons (with perhaps a procedure to handle spectators), it is crucial to introduce departures from this picture at low energy: off-shell character of the nucleons, geometrical spectators and participants, formation of compound nucleus, and progressive appearance of pre-equilibrium processes. We show that all these features can be taken care of with individual nucleons and by using criteria involving geometry and the four-momenta of the nucleons. Even more, the results displayed in Sec. IV testify to the success of this procedure. Of course, rather global quantities have been considered and the model should be tested also on double-differential cross sections. But the results accumulated up to now are very encouraging. We want to draw attention to the importance of this potentiality of the model for technical applications. In a thick target bombarded by a high-energy beam, many secondary reactions will be induced by clusters produced in primary interactions.

We hope to have shown that the improvement of our INCL model, from INCL4.2 to INCL4.6, has generated a powerful tool for the description of nucleon and light-cluster-induced reactions in a large domain of incident energy spanning from a few tens of MeV to 3 GeV. We stress that this description is based on a single microscopic cascade model, even if some ad hoc prescriptions have been added, as we discuss in detail. This addition has been made to improve the predictive power of the model in view of applications to thick spallation targets. Actually, the model is already included as an option in the GEANT4 [4], MCNPX [129], and PHITS [130] transport codes. Nevertheless, we think that the model is still prone to further improvement. We mentioned in this paper several results which are not sufficiently satisfactory, like for instance the yield of isotopes close to the target, which have large cross sections and whose accurate predictions are important for applications. We are currently working on such topics.

APPENDIX

Parametrization of R_{Coul}

The quantity R_{Coul} (in fm), defined in Sec. II D 4, is parametrized as

$$R_{\text{Coul}} = \frac{1.44 z Z_T}{a A_T^{2/3} - b} - c, \qquad \text{(A1)}$$

where z is the charge of the incident particle. The values of the quantities a, b, and c are provided in Table V.

This is valid for target mass number $A_T \geqslant 10$. For $A_T < 10$, $R_{\text{Coul}} = R_{\max}$ [see Eq. (2)]. The last equality also holds for incident protons and pions.

TABLE V. Values of the parameters a, b, c.

Incident particle	a	b	c
d	0.2565	0.78	2.5
t	0.2504	0.58	0.5
^{3}He	0.5009	1.16	0.5
^{4}He	0.5939	1.64	0.5

[1] D. Filges and F. Goldenbaum, *Handbook of Spallation Research Theory, Experiments and Applications* (Wiley VCH, Berlin, 2010).

[2] W. Gudowski, Nucl. Phys. A **654**, 436c (1999).

[3] H. Abderrahim, P. Baeten, D. De Bruyn, J. Heyse, P. Schuurmans, and J. Wagemans, Nucl. Phys. News **20**, 24 (2010).

[4] S. Agostinelli *et al.* (for the Geant4 Collaboration), Nucl. Instr. Meth. Phys. Res. A **506**, 250 (2003).

[5] I. Tanihata, in *Treatise on Heavy-Ion Science*, edited by D. A. Bromley, Vol. 8 (Plenum Press, New York, 1989).

[6] M. Durante, Riv. Nuovo Cimento Soc. Ital. Fis. **25**(8), 1 (2002).

[7] M. Longair, *High Energy Astrophysics* (Cambridge University Press, Cambridge, UK, 1997), Vols. 1 and 2.

[8] G. Kraft, Strahlenther. Onkol. **166**(1), 10 (1990).

[9] HINDAS Detailed final report, 2005 edited by J.-P. Meulders *et al.*, http://www.theo.phys.ulg.ac.be/wiki/index.php/Cugnon_Joseph.

[10] EUROTRANS/NUDATRA project EU Contract FI6W-CT-2004-516529, http://www.nupecc.org/presentations/IPEurotrans041112.pdf.

[11] A. Boudard, J. Cugnon, S. Leray, and C. Volant, Phys. Rev. C **66**, 044615 (2002).

[12] J.-J. Gaimard and K.-H. Schmidt, Nucl. Phys. A **531**, 709 (1991).

[13] A. R. Junghans, M. de Jong, H. G. Clerc, A. V. Ignatyuk, G. A. Kudyaev, and K.-H. Schmidt, Nucl. Phys. A **629**, 635 (1998).

[14] J. Benlliure, A. Grewe, M. de Jong, K.-H. Schmidt, and S. Zhdanov, Nucl. Phys. A **628**, 458 (1998).

[15] A. Boudard, J. Cugnon, S. Leray, and C. Volant, Nucl. Phys. A **740**, 195 (2004).

[16] B. Rapp, J.-C. David, V. Blideanu, D. Doré, D. Ridikas, and N. Thiollière, in *Proceedings of International Workshop on Shielding Aspects of Accelerators, Targets and Irradiation Facilities (SATIF-8)*, NEA Report NEA/NSC/DOC(2010)6, p. 251, 2010.

[17] *Benchmark of Spallation Models*, organized by the IAEA, http://www-nds.iaea.org/spallations.

[18] J. Cugnon, A. Boudard, S. Leray, and D. Mancusi, *Proc. of Int. Topical Meeting on Nuclear Research Applications and Utilization of Accelerators (AccApp09), IAEA, Vienna, 2009* (IAEA Publications, Vienna, 2010), ISBN 978-92-0-150410-4, SM/SR-02, 8p.

[19] J.-C. David, D. Filges, F. Gallmeier, M. Khankader, A. Konobeyev, S. Leray, G. Mank, A. Mengoni, R. Michel, N. Otuka, and Y. Yariv, *Proc. of Joint International Conference on Supercomputing in Nuclear Applications and Monte Carlo 2010 (SNA + MC2010), Japan, 2010*, in Progress in NUCLEAR SCIENCE and TECHNOLOGY, Vol. 2, 942 (2011).

[20] W. Botermans and R. Malfliet, Phys. Lett. B **171**, 22 (1986).

[21] W. Botermans and R. Malfliet, Phys. Rep. **198**, 115 (1990).

[22] V. E. Bunakov and G. V. Matvejev, Z. Phys. A: At. Nucl. **322**, 511 (1985).

[23] G. Welke, R. Malfliet, C. Grégoire, M. Prakash, and E. Suraud, Phys. Rev. C **40**, 2611 (1989).

[24] J. Cugnon, Few-Body Syst. **53**, 181 (2012).

[25] J. Cugnon and P. Henrotte, Eur. Phys. J. A **16**, 393 (2003).

[26] P. E. Hodgson, *The Nucleon Optical Potential* (World Scientific, Singapore, 1994).

[27] J.-P. Jeukenne, A. Lejeune, and C. Mahaux, Phys. Rep. **25**, 83 (1976).

[28] J.-P. Jeukenne, C. Mahaux, and R. Sartor, Phys. Rev. C **43**, 2211 (1991).

[29] T. Aoust and J. Cugnon, Eur. Phys. J. A **21**, 79 (2004).

[30] T. Aoust and J. Cugnon, Nucl. Phys. A **828**, 52 (2009).

[31] A. M. Lane, Phys. Rev. Lett. **8**, 171 (1962).

[32] T. Aoust and J. Cugnon, Phys. Rev. C **74**, 064607 (2006).

[33] J. Cugnon, A. Boudard, J.-C. David, A. Kelić-Heil, S. Leray, D. Mancusi, and M. V. Ricciardi, J. Phys.: Conf. Ser. **312**, 082019 (2011).

[34] P. Henrotte, Ph.D. thesis, University of Liège, 2005 (unpublished).

[35] A. Boudard, in *Proc. of the Int. Conf. on Nuclear Data for Science and Technology 2007*, edited by O. Bersillon *et al.* (EDP Sciences, Les Ulis, France, 2008), pp. 1103–1108.

[36] Y. Yariv and Z. Fraenkel, Phys. Rev. C **20**, 2227 (1979).

[37] Y. Yariv and Z. Fraenkel, Phys. Rev. C **24**, 488 (1981).

[38] Y. Yariv, T. Aoust, A. Boudard, J. Cugnon, J.-C. David, S. Lemaire, and S. Leray, in *Proc. of the Int. Conf. on Nuclear Data for Science and Technology 2007*, edited by O. Bersillon *et al.* (EDP Sciences, Les Ulis, France, 2008), pp. 1125–1128.

[39] A. Boudard, J. Cugnon, P. Kaitaniemi, S. Leray, and D. Mancusi, in *Proc. of Int. Topical Meeting on Nuclear Research Applications and Utilization of Accelerators (AccApp09)* (IAEA Publications, Vienna, 2010), ISBN 978-92-0-150410-4, AP/IE-08, 8p.

[40] P. Kaitaniemi, A. Boudard, S. Leray, J. Cugnon, and D. Mancusi (on behalf of the Geant4 Collaboration), *Joint International Conference on Supercomputing in Nuclear Applications and Monte Carlo 2010 (SNA + MC2010), Japan, 2010*, in Progress in NUCLEAR SCIENCE and TECHNOLOGY, Vol. 2, 788 (2011).

[41] A. S. Goldhaber, Phys. Lett. B **53**, 306 (1974).

[42] H. Feshbach and K. Huang, Phys. Lett. B **47**, 300 (1973).

[43] J. Hüfner and M. C. Nemes, Phys. Rev. C **23**, 2538 (1981).

[44] Y. Aoki, N. Okumura, T. Joh, N. Takahashi, and Y. Honkyu, Nucl. Phys. A **673**, 189 (2000).

[45] H. W. Bertini, Phys. Rev. **131**, 1801 (1963).

[46] H. W. Bertini, Phys. Rev. **188**, 1711 (1969).

[47] K. K. Gudima, S. G. Mashnik, and V. D. Toneev, Nucl. Phys. A **401**, 329 (1983).

[48] S. G. Mashnik and A. J. Sierk, in *Proc. of Int. Conf. on Nuclear Data for Science and Technology, Tsukuba (Japan), 2001*, in Journal of Nuclear Science and Technology, Supplement 2, 720, 2002; and Los Alamos preprint LANL Report LA-UR-01-5390.

[49] Z. Rudy and A. Kowalczyk, *Joint ICTP-IAEA Advanced Workshop on Model Codes for Spallation Reactions, in IAEA INDC (NDS)-0530*, edited by D. Filges *et al.* (IAEA Publications, Vienna, 2008), pp. 53–64.

[50] C. Hartnack *et al.*, Eur. Phys. J. A **1**, 151 (1998).

[51] K. Niita, S. Chiba, Toshiki Maruyama, Tomoyuki Maruyama, H. Takada, T. Fukahori, Y. Nakahara, and A. Iwamoto, Phys. Rev. C **52**, 2620 (1995).

[52] D. Filges, S. Leray, Y. Yariv, A. Mengoni, A. Stanculescu, and G. Mank, *Joint ICTP-IAEA Advanced Workshop on Model Codes for Spallation Reactions, IAEA INDC (NDS)-0530* (IAEA Publications, Vienna, 2008).

[53] A. Kelić, M. V. Ricciardi, and K.-H. Schmidt, in *Joint ICTP-IAEA Advanced Workshop on Model Codes for Spallation Reactions*, in IAEA INDC (NDS)-0530, edited by D. Filges *et al.* (IAEA Publications, Vienna, 2008), pp. 181–222.

[54] R. F. Carlson, At. Data Nucl. Data Tables **63**, 93 (1996).

[55] R. E. Prael and M. B. Chadwick, preprint Los Alamos National Laboratory LA-UR-97-1744, 1997.

[56] B. C. Barashenkov, *Cross Sections of Interactions of Particles and Nuclei with Nuclei* (OIYaI, Dubna, 1993) [in Russian].

[57] R. K. Tripathi, J. W. Wilson, and F. A. Cucinotta, Nucl. Instrum. Methods Phys. Res., Sect. B **173**, 391 (2001).

[58] S. Leray *et al.*, Phys. Rev. C **65**, 044621 (2002).

[59] X. Ledoux *et al.*, Phys. Rev. Lett. **82**, 4412 (1999).

[60] E. L. Hjort *et al.*, Phys. Rev. C **53**, 237 (1996).

[61] A. Guertin *et al.*, Eur. Phys. J. A **23**, 49 (2005).

[62] F. E. Bertrand and R. W. Peelle, Phys. Rev. C **8**, 1045 (1973).

[63] EXFOR/CSISRS, National Nuclear Data Center, http://www.nndc.bnl.gov/exfor/exfor00.htm.

[64] A. Budzanowski *et al.*, Phys. Rev. C **80**, 054604 (2009).

[65] R. E. Chrien *et al.*, Phys. Rev. C **21**, 1014 (1980).

[66] J. A. McGill, G. W. Hoffmann, M. L. Barlett, R. W. Fergerson, E. C. Milner, R. E. Chrien, R. J. Sutter, T. Kozlowski, and R. L. Stearns, Phys. Rev. C **29**, 204 (1984).

[67] A. Budzanowski *et al.*, Phys. Rev. C **78**, 024603 (2008).

[68] J. Franz *et al.*, Nucl. Phys. A **828**, 774 (1990).

[69] A. A. Cowley *et al.*, Phys. Rev. C **54**, 778 (1996).

[70] A. Bubak *et al.*, Phys. Rev. C **76**, 014618 (2007).

[71] A. Letourneau *et al.*, Nucl. Phys. A **712**, 133 (2002).

[72] C.-M. Herbach *et al.*, Nucl. Phys. A **765**, 426 (2006).

[73] S. Leray, A. Boudard, J. Cugnon, J.-C. David, A. Kelià-Heil, D. Mancusi, and M. V. Ricciardi, Nucl. Instrum. Methods Phys. Res., Sect. B **268**, 581 (2010).

[74] H. Machner *et al.*, Phys. Rev. C **73**, 044606 (2006).

[75] J.-C. David, A. Boudard, J. Cugnon, S. Leray, and D. Mancusi, FP7_ANDES report/Task 4.1/Deliverable 4.1, 2011, available at http://www.andes-nd.eu.

[76] D. R. F. Cochran *et al.*, Phys. Rev. D **6**, 3085 (1972).

[77] T. Enqvist *et al.*, Nucl. Phys. A **686**, 481 (2001).

[78] A. Kelić-Heil (private communication).

[79] C. Villagrasa-Canton *et al.*, Phys. Rev. C **75**, 044603 (2007).

[80] B. Fernández-Domínguez *et al.*, Nucl. Phys. A **747**, 227 (2005).

[81] L. Audouin *et al.*, Nucl. Phys. A **768**, 1 (2006).

[82] J. Taïeb *et al.*, Nucl. Phys. A **724**, 413 (2003).

[83] M. Bernas *et al.*, Nucl. Phys. A **725**, 213 (2003).

[84] M. Bernas *et al.*, Nucl. Phys. A **765**, 197 (2006).

[85] M. V. Ricciardi *et al.*, Phys. Rev. C **73**, 014607 (2006).

[86] D. Mancusi, A. Boudard, J. Cugnon, J.-C. David, T. Gorbinet, and S. Leray, Phys. Rev. C **84**, 064615 (2011).

[87] Y. Tall *et al.*, in *Proceedings of the International Conference on Nuclear Data for Science and Technology, 2007, Nice, France*, edited by O. Bersillon, F. Gunsing, E. Bauge, R. Jacqmin, and S. Leray (EDP Sciences, Les Ulis, France, 2008), p. 1069.

[88] S. G. Mashnik *et al.*, J. Phys.: Conf. Ser. **41**, 340 (2006).

[89] S. Leray *et al.*, Journal of the Korean Physical Society **59**, 791 (2011).

[90] A. Ingemarsson *et al.*, Nucl. Phys. A **676**, 3 (2000).

[91] A. Ingemarsson *et al.*, Nucl. Phys. A **696**, 3 (2001).

[92] G. Igo and B. D. Wilkins, Phys. Rev. **131**, 1251 (1963).

[93] A. Auce *et al.*, Phys. Rev. C **50**, 871 (1994).

[94] A. Auce *et al.*, Phys. Rev. C **53**, 2919 (1996).

[95] L. V. Dubar, O. F. Nemets, L. I. Slyusarenko, and V. V. Tokarevskij, Yad. Fiz. **20**, 624 (1974).

[96] S. Mayo, W. Schimmerling, R. M. Sametband, and R. M. Eisberg, Nucl. Phys. **62**, 393 (1965).

[97] K. Bearpark, W. R. Graham, and G. Jones, Nucl. Phys. **73**, 206 (1965).

[98] A. Budzanowski, L. Freindl, K. Grotowski, M. Rzeszutko, M. Sỹÿapa, J. Szmider, and P. E. Hodgson, Nucl. Phys. **49**, 144 (1963).

[99] G. P. Millburn *et al.*, Phys. Rev. **95**, 1268 (1954).

[100] D. Ridikas, W. Mittig, and J. A. Tostevin, Phys. Rev. C **59**, 1555 (1999).

[101] J. A. Tostevin, S. Rugmai, and R. C. Johnson, Phys. Rev. C **57**, 3225 (1998).

[102] H. Okamura *et al.*, Phys. Lett. B **325**, 308 (1994).

[103] M. Avrigeanu, V. Avrigeanu, and A. J. Koning, Phys. Rev. C **85**, 034603 (2012).

[104] E. Šimečková *et al.*, Phys. Rev. C **84**, 014605 (2011).

[105] A. R. Barnett and J. S. Lilley, Phys. Rev. C **9**, 2010 (1974).

[106] A. Hermanne, F. Tárkányi, S. Takács, Z. Szücs, Yu. N. Shubin, and A. I. Dityuk, Appl. Radiat. Isot. **63**, 1 (2005).

[107] I. A. Rizvi, M. K. Bhardwaj, M. Afzal Ansari, and A. K. Chaubey, Appl. Radiat. Isot. **41**, 215 (1990).

[108] J.-P. Didelez, R. M. Lieder, H. Beuscher, D. R. Haenni, H. Machner, M. Müller-Veggian, and C. Mayer-Böricke, Nucl. Phys. A **341**, 421 (1980).

[109] E. T. Chulick and J. B. Natowitz, Nucl. Phys. A **173**, 487 (1971).

[110] R. Bass, Nucl. Phys. A **231**, 45 (1974).

[111] W. J. Ramler, J. Wing, D. J. Henderson, and J. R. Huizenga, Phys. Rev. **114**, 154 (1959).

[112] E. L. Kelly and E. Segrè, Phys. Rev. **75**, 999 (1949).

[113] N. E. Scott, J. W. Cobble, and P. J. Daly, Nucl. Phys. A **119**, 131 (1968).

[114] S. Mrówczyński, Phys. Rev. D **36**, 1520 (1987).

[115] D. Trautmann, G. Baur, and F. Rösel, J. Phys. B **16**, 3005 (1983).

[116] J. Cugnon and D. Vautherin, in *Proc. of the Int. Workshop Hadronic Atoms and Positronium in the Standard Model*, edited by M. A. Ivanov, A. Arbuzov, E. Kuraev, V. Lyubovitskij, and A. Rusetsky (JINR Publications, Dubna, 1998), ISBN 5-85165-514-3, pp. 128–134.

[117] P. H. Stelson and F. K. McGowan, Phys. Rev. B **133**, 911 (1964).

[118] S. Yanagita, K. Yamakoshi, and R. Gensho, Nucl. Phys. A **303**, 254 (1978).

[119] V. N. Levkovskij, *Activation Cross Sections for Nuclides of Average Masses (A = 40–100) by Protons and Alpha-Particles with Average Energies (E = 10–50 MeV)* (Inter Vesi, Moscow, 1991).

[120] A. Yadav *et al.*, Phys. Rev. C **78**, 044606 (2008).

[121] S. Tanaka, J. Phys. Soc. Jpn. **15**, 2159 (1960).

[122] A. Fenyvesia, F. Tárkányia, and S.-J. Heselius, Nucl. Instrum. Methods Phys. Res., Sect. B **222**, 355 (2004).

[123] F. Szelecsényia, Z. Kovácsa, K. Suzukib, K. Okadab, T. Fukumurab, and K. Muka, Nucl. Instrum. Methods Phys. Res., Sect. B **222**, 364 (2004).

[124] E. A. Bryant, D. R. F. Cochran, and J. D. Knight, Phys. Rev. **130**, 1512 (1963).

[125] M. Cogneau, L. J. Gilly, and J. Cara, Nucl. Phys. A **99**, 686 (1967).

[126] G. Folger, V. N. Ivanchenko, and H. P. Wellisch, Eur. Phys. J. A **21**, 407 (2004).

[127] H. Kumawat and V. S. Barashenkov, Eur. Phys. J. A **26**, 61 (2005).

[128] Yu. E. Titarenko *et al.*, Phys. Rev. C **84**, 064612 (2011).

[129] D. B. Pelowitz *et al.*, MCNPX 2.7.E extensions, Los Alamos Report LA-UR-11-01502, 2011.

[130] K. Niita *et al.*, PHITS: Particle and Heavy Ion Transport code System, Version 2.23, JAEA-Data/Code 2010-022, 2010.